

5 Zero Set of the Order Parameter, Especially in Rings

Jorge Berger

Ort Braude College, 21982 Karmiel, Israel

Abstract We discuss the conditions and the positions where the order parameter vanishes in a multiply connected sample. The first sections are extensions of the de Gennes–Alexander formalism, but most of the chapter deals with samples of finite width. There are several surprising predictions, e.g.: a vortex can be much thinner than the coherence length, and its position may radically change with the fluxoid number; there are critical points inside the superconducting area in the phase diagram. Experimental verification is proposed.

5.1 Introduction: The Price of Connectivity

The behavior of superconductors can be described by means of the Ginzburg–Landau (GL) formalism. This formalism was reviewed in Sections 1.2 and 2.1.1, but in order to introduce our notation we rewrite the starting equations. According to this formalism, the equilibrium magnetic potential and the superconducting order parameter are such that they minimize the GL potential

$$G = \int \left[\mu(-|\psi|^2 + |\psi|^4/2) + |(i\nabla - \tilde{\mathbf{A}})\psi|^2 \right] + (\kappa^2/\mu) \int |\nabla \times \tilde{\mathbf{A}} - 2\pi\mathbf{H}_e/\Phi_0|^2. \quad (5.1)$$

Here $\psi = |\psi|e^{i\varphi}$ is the order parameter, with the normalization introduced after (2.4), \mathbf{H}_e is the applied field, Φ_0 the quantum of flux and κ the GL parameter; μ is an abbreviation for ξ^{-2} , where ξ is the coherence length, and $\tilde{\mathbf{A}} = 2\pi\mathbf{A}/\Phi_0$, with \mathbf{A} the magnetic potential. The first integral in (5.1) is over the sample volume and the second integral is over the entire space. Note that in many sources $\tilde{\mathbf{A}}$ appears with the opposite sign; these sources disregard the awkward fact that the electron charge is negative. The normalizations in (5.1) take for granted that the temperature is below T_c , the normal/superconducting transition temperature when no magnetic field is applied.

The first GL equation is obtained by minimizing G with respect to ψ . Variation gives

$$(i\nabla - \tilde{\mathbf{A}})^2\psi = \mu(1 - |\psi|^2)\psi \quad (5.2)$$

inside the sample, with the boundary requirement that the normal component of $(i\nabla - \tilde{\mathbf{A}})\psi$ vanishes. The second GL equation (obtained by minimizing G w.r.t. \mathbf{A}) is not required when the sample is very thin compared to $\kappa\xi$, and will be postponed until Section 5.4.1.

Inspection of the Ginzburg–Landau potential G shows that it contains only two terms that depend on the phase φ , and both are non-negative: $|(i\nabla - \tilde{\mathbf{A}})\psi|^2$,

which can be further decomposed into $(\nabla|\psi|)^2 + |(\nabla\varphi + \tilde{\mathbf{A}})\psi|^2$, and H_i^2 , with $\mathbf{H}_i = \nabla \times \mathbf{A} - \mathbf{H}_e$. It is therefore clear that, if there is some φ such that the φ -dependent terms vanish, this φ will be the most appropriate candidate for minimization.

One situation in which this happens is when the applied field vanishes within the sample: then we can pick φ such that $\nabla\varphi = -\tilde{\mathbf{A}}$. (In this case, the current, H_i and the total field also vanish.) This case is considered in detail in Chapter 3. Another opportunity like this appears when the sample is a narrow wire (or a narrow shell parallel to the magnetic field), as in Fig. 5.1. Since the normal component of $(i\nabla - \tilde{\mathbf{A}})\psi$ is required to vanish at the boundary, in the case of a thin wire we may take this component as negligible everywhere, so that we only have to require that the tangential component vanishes too. This is achieved if

$$\varphi(s') - \varphi(s) = - \int_s^{s'} \tilde{\mathbf{A}} \cdot d\mathbf{r}, \quad (5.3)$$

where s is the arc length and the integration is performed along the wire. Again, we get rid of the two phase dependent terms and are left with a minimization over $|\psi|$ only.

However, let us imagine that we fill the gap between a and a' with superconducting material. Instead of enhancing superconductivity, we add a constraint: $\psi(a)$ and $\psi(a')$, and in particular their phases (up to a multiple of 2π), must be the same. The minimizer of the unconstrained problem may therefore be ruled out, and superconductivity will have to compromise to a minimizer in the set $\{\psi(a') = \psi(a)\}$. This means that connectivity is a thermodynamic burden. Our question is whether there are cases in which superconductivity – and therefore connectivity – are broken at some place in order to get rid of this burden.

Sections 5.2–5.4 consider situations in increasing order of generality in the following sense: in Section 5.2, wires are thin and have uniform (or piecewise

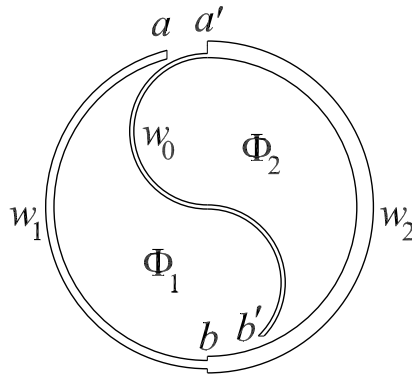


Figure 5.1. A narrow superconducting wire, with several possible connectivities. The three branches have the same length L and their cross sections are w_0 , w_1 and w_2

uniform) cross sections; in Section 5.3, cross sections will be nonuniform and, in Section 5.4, wires will turn into wide surfaces. However, the formalisms of each section are quite independent, so that their consecutive reading is not essential.

5.2 The de Gennes-Alexander (dGA) Approach

The easiest situation for evaluation of the price of connectivity is provided by the dGA case, since the differential equations have already been integrated. The dGA formalism is applicable to networks of thin branches with constant cross section, at a bifurcation from the normal state. For further simplicity, we shall consider cases in which all the branches have the same length, L . Since the free energy decreases with μ , minimization of the free energy is translated here into minimization of the value of μ for which there is a non trivial solution.

Our analysis will be based on Chapter 2, but a word of warning is required. The solution of (2.16) is

$$\psi(s) = \exp(-i\gamma(s))[k_1 \exp(i\sqrt{\mu}s + k_2 \exp(-i\sqrt{\mu}s)] \quad (5.4)$$

where γ is the integral in (5.3) (without the $-$ sign) and k_1 and k_2 are constants, which are chosen to comply with the values of ψ at the extremes of the branch, $s = 0$ and $s = L$. In general, these are 2 independent conditions and we obtain (2.19); but, if $\sqrt{\mu}L = \pi$ or $\sqrt{\mu}L = 0$, then we obtain a condition for $\psi(L)/\psi(0)$:

$$\psi(L) \exp(i\gamma(L))/\psi(0) = 1 \quad \sqrt{\mu}L = 0 \quad (5.5a)$$

$$\psi(L) \exp(i\gamma(L))/\psi(0) = -1 \quad \sqrt{\mu}L = \pi . \quad (5.5b)$$

If (5.5a) or (5.5b) is fulfilled, there is a family of degenerate solutions. Note that $\sqrt{\mu}L$ is non negative by definition and will never be greater than π , since we can always find a smaller μ with the same value of $\cos(\sqrt{\mu}L)$. If (2.19) is valid, the condition for having a point where $\psi(s) = 0$ along the branch $0 < s < L$ is

$$\psi(L) \exp(i\gamma(L))/\psi(0) < 0 . \quad (5.6)$$

It is interesting to compare this with (5.5b).

5.2.1 One Loop

Figure 5.1 with $a' = a$ has three nodes: b' , a and b . The Alexander nodal equations (2.21), after elimination of $\psi(b')$, become

$$[(w_0 + w_1 + w_2)X - w_0/X] \psi(a) - (w_1 e^{i\gamma_1} + w_2 e^{-i\gamma_2}) \psi(b) = 0 , \quad (5.7a)$$

$$-(w_1 e^{-i\gamma_1} + w_2 e^{i\gamma_2}) \psi(a) + (w_1 + w_2)X \psi(b) = 0 , \quad (5.7b)$$

where X is shorthand for $\cos(\sqrt{\mu_0}L)$, w_i is the cross section of branch i and γ_i is $\gamma(L)$ evaluated along this branch in the positive mathematical sense; μ_0 is the

lowest eigenvalue of this system of equations and gives the value of μ at which the bifurcation from the normal state occurs. Here,

$$\cos(\sqrt{\mu_0}L) = ([w_0 + |w_1 e^{i(\gamma_1 + \gamma_2)} + w_2|^2 / (w_1 + w_2)] / (w_0 + w_1 + w_2))^{1/2}. \quad (5.8)$$

Let us now investigate under what conditions ψ vanishes at some point in the branches 1 or 2. From (5.7b), $\psi(b)e^{i\gamma_1} / \psi(a) < 0$ would require $w_1 < w_2$ together with $e^{i(\gamma_1 + \gamma_2)} = -1$, which occurs when the flux $\Phi_1 + \Phi_2$ is an integer plus half number of quanta Φ_0 . The same analysis can be repeated for branch 2. $\psi(b)$ would vanish if $w_1 = w_2$ and $e^{i(\gamma_1 + \gamma_2)} = -1$. For $w_0 > 0$, $\psi(a)$ can never vanish for the lowest eigenvalue. In summary, there is a zero in the order parameter only when the flux enclosed by the circle is an integer plus half, and then the zero appears at the thinner branch. In the symmetric case, the zero appears at the point opposite to the branch ab' . At the branch ab' itself, it is easily seen that $\psi(b')e^{i\gamma_0} / \psi(a) > 0$ and the phase obeys (5.3) along the entire branch, as is physically obvious from the fact that this branch carries no current.

We know already that, for appropriate flux, ψ vanishes somewhere in the thinner outer branch. Let us now check the following: could there be a situation where it is thermodynamically favorable for superconductivity to spontaneously break the connectivity in order to allow (5.3) to be fulfilled everywhere, even though the dGA formalism does not require ψ to vanish? In other words, would it pay to replace the constraint that the sample encloses a given flux by the constraint that ψ has to vanish at some point? The answer seems to be negative: if $e^{i(\gamma_1 + \gamma_2)} = -1$, then both constraints are compatible and the solutions coincide; changing $e^{i(\gamma_1 + \gamma_2)}$ to a different value will cause μ_0 in (5.8) to decrease (dGA case), whereas the case with broken connectivity is insensitive to the flux and remains at its high value.

Actually, ψ does not have to vanish in order to cope with the price of connectivity. It is enough that ψ be small in some region to enable a fast change of φ in that region at a low energy price. In [6] it is found that this price is proportional to the minimum of $|\psi|$ (provided that this minimum is small).

The case of a loop without the extra branch is obtained if we set $w_0 = 0$. The expression for the eigenvalue now takes the simpler form

$$\cos(\sqrt{\mu_0}L) = |w_1 e^{i(\gamma_1 + \gamma_2)} + w_2| / (w_1 + w_2).$$

The conclusions remain qualitatively the same, except that now, for $w_1 = w_2$ and $\gamma_1 + \gamma_2 = \pi \pmod{2\pi}$, $\cos(\sqrt{\mu_0}L) = 0$ and $\psi(a)$ and $\psi(b)$ are undetermined.

5.2.2 Two Loops

Let us now increase the connectivity in Fig. 5.1 by connecting also b and b' . There are now two nodes, and Alexander's equation becomes

$$(w_0 + w_1 + w_2)X\psi(a) - (w_0 e^{i\gamma_0} + w_1 e^{i\gamma_1} + w_2 e^{-i\gamma_2})\psi(b) = 0, \quad (5.9a)$$

$$-(w_0 e^{-i\gamma_0} + w_1 e^{-i\gamma_1} + w_2 e^{i\gamma_2})\psi(a) + (w_0 + w_1 + w_2)X\psi(b) = 0; \quad (5.9b)$$

μ_0 is given by

$$\cos(\sqrt{\mu_0}L) = |w_0e^{i\gamma_0} + w_1e^{i\gamma_1} + w_2e^{-i\gamma_2}|/(w_0 + w_1 + w_2) .$$

The value of μ_0 here is generically greater than in (5.8), as expected from the larger connectivity. From (5.9b) we see that, except for a positive factor,

$$\psi(b)e^{i\gamma_0}/\psi(a) \propto (w_0 + w_1e^{i(\gamma_0-\gamma_1)} + w_2e^{i(\gamma_0+\gamma_2)}) .$$

For simplicity, let us consider the case $\Phi_1 = \Phi_2 = \phi\Phi_0$, so that

$$\psi(b)e^{i\gamma_0}/\psi(a) \propto (w_0 + w_1e^{2\pi i\phi} + w_2e^{-2\pi i\phi})$$

and, similarly,

$$\psi(b)e^{i\gamma_1}/\psi(a) \propto (w_0e^{-2\pi i\phi} + w_1 + w_2e^{-4\pi i\phi}) ,$$

$$\psi(b)e^{-i\gamma_2}/\psi(a) \propto (w_0e^{2\pi i\phi} + w_1e^{4\pi i\phi} + w_2) .$$

If $w_1 \neq w_2$, we see that (5.6) can be fulfilled only if ϕ is an integer plus half. In this case, ψ will have a zero in the inner branch if $w_0 < w_1 + w_2$ and will have zeros at both outer branches if $w_0 > w_1 + w_2$. In the symmetric case $w_1 = w_2$, there is a zero in the middle branch for the entire region $\cos(2\pi\phi) < -w_0/(w_1 + w_2)$.

We see that there is a qualitative difference between the symmetric case here (or, say, the case of the double yin-yang in Section 2.2.2), where there is a zero at a fixed position for a finite region of ϕ , and the nonsymmetric case, or the case of the single loop, where zeros are present for isolated values of ϕ . In the first cases, the zero may be regarded as a consequence of a geometric symmetry; in the latter cases, it may be regarded as a consequence of the symmetry of Alexander's equation under the transformation $\psi(a) \rightarrow \overline{\psi(a)}$, $\psi(b) \rightarrow e^{-2i\gamma_0}\overline{\psi(b)}$, where the overline denotes complex conjugation.

5.3 Perturbational Approach

In this section we still deal with a wire (or shell) which is sufficiently narrow, so that ψ will depend only on the arc length and the induced field will be neglected. We first develop a formalism that will enable us to extend the dGA method to samples with nonuniform width and beyond the onset of superconductivity.

For a narrow wire, the boundary condition that the normal component of $\text{Re}[\overline{\psi}(i\nabla - \tilde{\mathbf{A}})\psi]$ vanishes may be replaced by the physical condition that the current

$$I = -w|\psi|^2(\varphi' + \tilde{A}) \quad (5.10)$$

will be constant along the wire. In Gaussian units, the current is $c\Phi_0\mu I/[2(2\pi\kappa)^2]$. Here $|\psi|$, φ and the cross section w are functions of the arc length s and $'$ denotes derivative with respect to it; \tilde{A} is the tangential component of $\tilde{\mathbf{A}}$. We can use (5.10) to eliminate φ from the free energy. This gives

$$G = \int \left[w \left(-\mu|\psi|^2 + \frac{\mu}{2}|\psi|^4 + (|\psi'|)^2 \right) + \frac{I^2}{w|\psi|^2} \right] ds , \quad (5.11)$$

from which we obtain the Euler-Lagrange equation

$$(w|\psi'|)' + w\mu(|\psi| - |\psi|^3) - I^2/(w|\psi|^3) = 0. \quad (5.12)$$

In this equation the absolute value of ψ has been isolated from its phase, which enters the equation only through the constant I . This form was used in [6]. However, for the purpose of extension to the case of finite width, we reintroduce φ . Introducing (5.10) into (5.12) gives

$$(w|\psi'|)' + w\mu(|\psi| - |\psi|^3) - w|\psi|(\varphi' + \tilde{A})^2 = 0. \quad (5.13)$$

In order to determine the two real functions $|\psi|$ and φ , we require an additional equation. This is obtained by taking the derivative of (5.10), which gives

$$w|\psi|(\varphi'' + \tilde{A}') + (\varphi' + \tilde{A})(2w|\psi'| + w'|\psi|) = 0. \quad (5.14)$$

It is interesting to note that in obtaining (5.13) and (5.14) we have not made any assumption as to the value of $\text{Im}[\bar{\psi}(i\nabla - \tilde{\mathbf{A}})\psi]$ at the boundary. This value controls the normal derivative of $|\psi|$, but since ψ has no room to vary anyway, this condition has no influence in the one dimensional limit.

It can be verified by direct evaluation that the system of equations (5.13) and (5.14) is equivalent to the complex equation

$$(i\partial_s - \tilde{A})^2\psi + (iw'/w)(i\partial_s - \tilde{A})\psi = \mu(\psi - |\psi|^2\psi), \quad (5.15)$$

which is obtained in [15] as the limiting case of a two dimensional problem.

In the following we shall be interested in a loop which encloses flux $\phi\Phi_0$. In this section we choose a gauge for which A is constant, define the perimeter as $2\pi R$ and $\theta = s/R$; we also redefine $'$ as derivative with respect to θ , and μ as $(R/\xi)^2$. With these adimensionalized definitions, (5.15) becomes

$$\mathcal{H}_0\psi + (iw'/w)(i\partial_\theta - \phi)\psi = \mu(\psi - |\psi|^2\psi), \quad (5.16)$$

with $\mathcal{H}_0 = (i\partial_\theta - \phi)^2$.

5.3.1 Uniform Cross Section

If we set $w' \equiv 0$ in (5.16), we find various solutions. One family is

$$\psi = \sqrt{1 - (m - \phi)^2/\mu} e^{-mi\theta}, \quad (5.17)$$

with m integer. A solution like this exists for $\mu \geq (m - \phi)^2$. Another family of solutions is

$$|\psi|^2 = q - (2n\nu^2/\mu) \text{cn}^2(\nu\theta, n), \quad (5.18)$$

with $\nu = K(n)/\pi$ (or a multiple of it), $q = (2/3)[1 + (2n - 1)\nu^2/\mu]$ and

$$\varphi = \sqrt{\frac{q}{8\mu}[\mu^2(q - 2)^2 - 4\nu^4]} \int_0^\theta \frac{d\theta'}{|\psi(\theta')|^2} - \phi\theta. \quad (5.19)$$

Here K is the elliptic integral and cn a Jacobian elliptic function. The value of n has to be such that either ψ vanishes at some place or $\varphi(2\pi) = \varphi(0) \pmod{2\pi}$. This family coalesces with a member of (5.17) for $n = 0$ and the case of broken connectivity is obtained for $(1+n)\nu^2 = \mu$. By continuously varying n and ϕ , and changing the value of $\varphi(2\pi) - \varphi(0)$ when connectivity is broken, it is possible to bridge continuously between solutions in (5.17) with different winding numbers m . The coalescence of families (5.17) and (5.18) occurs at the lines $6(\phi - m)^2 - 2\mu = 1$. The region $n < 0$ does not give new solutions. For additional families of solutions and cases in which $\nu = iK(1-n)/\pi$, see [4]. Clearly, it is always possible to add constants to θ and to φ .

Solutions in family (5.17) are local minima of G for $6(\phi - m)^2 - 2\mu < 1$ and saddle points beyond this range [13]; a numerical search indicates that solutions in family (5.18), and in particular the solution that breaks connectivity, are never local minima.

5.3.2 Weakly Nonuniform Cross Section

We saw that for the case of uniform cross section connectivity is never broken. However, we shall see that small deviations from uniformity generically stabilize broken connectivity.

Using (5.17), (5.11) and (5.10), we find that the free energy increases with $|\phi - m|$, so that for $\phi = m + 1/2$ there will be a degenerate ground state, since the states with winding numbers m and $m + 1$ share the lowest free energy. We want to analyze what happens near this situation and therefore write $\phi = m + 1/2 + \epsilon\phi_1$, where ϵ will be our parameter of smallness. For the shape of the cross section we write

$$w(\theta) = w_0 \left(1 + \frac{\epsilon}{2} \sum_{j \neq 0} \beta_j e^{ji\theta} \right), \quad (5.20)$$

where w_0 is the average width and $\beta_{-j} = \bar{\beta}_j$. We will limit this study to the region close to the onset of superconductivity; more precisely, we require $|\psi|$ to be at most of order $\epsilon^{1/2}$. For $\phi = m + 1/2$ and uniform cross section, this onset occurs at $\mu = 1/4$ and we therefore write $\mu = 1/4 + \epsilon\mu_1$.

We rewrite (5.16) in the form

$$(\mathcal{H}_0 + V)\psi = \mu\psi \quad (5.21)$$

where \mathcal{H}_0 is now $(i\partial_\theta - m - 1/2)^2$ and

$$V = -2i[\phi - (m + \frac{1}{2})]\partial_\theta + \phi^2 - (m + \frac{1}{2})^2 + \frac{iw'}{w}(i\partial_\theta - \phi) + \mu|\psi|^2.$$

Equation (5.21) is not linear, since V involves $|\psi|$, which will have to be determined self consistently. Since in the limit $\epsilon \rightarrow 0$ (5.21) is linear and its general groundstate is any linear combination of $e^{-mi\theta}$ and $e^{-(m+1)i\theta}$, we write

$$\psi = \epsilon^{1/2}\eta(e^{-mi\theta} + ge^{-(m+1)i\theta}) + \epsilon^{3/2}\psi_1, \quad (5.22)$$

where, without loss of physical generality, we may take η real and non negative. Keeping only terms to $O(\epsilon)$, V becomes

$$V = \epsilon \left\{ (2\phi_1 + \frac{1}{2} \sum j\beta_j e^{j i \theta})(-i\partial_\theta + m + \frac{1}{2}) + \frac{\eta^2}{4} |1 + g e^{-i\theta}|^2 \right\}. \quad (5.23)$$

Substituting (5.22) and (5.23) into (5.21), collecting the coefficients of $e^{-mi\theta}$ and $e^{-(m+1)i\theta}$ and using $\eta \neq 0$ we obtain

$$\begin{aligned} \phi_1 - \mu_1 + \frac{\eta^2}{4}(1 + 2|g|^2) &= \frac{1}{4}\beta_1 g, \\ -\phi_1 - \mu_1 + \frac{\eta^2}{4}(2 + |g|^2) &= \frac{1}{4}\frac{\bar{\beta}_1}{g}. \end{aligned} \quad (5.24)$$

From here we learn that only the first harmonic of the shape of $w(\theta)$ is important and that $\beta_1 g$ is real. The temperature for the onset of superconductivity is obtained by setting $\eta \rightarrow 0$ and taking the lowest solution in (5.24). This gives $\mu = 1/4 - \sqrt{\phi_1^2 + |\beta_1|^2/16}$.

From (5.24), it is easy to express ϕ_1 and η as functions of $|g|$:

$$\begin{aligned} \frac{\phi_1}{|\beta_1|} &= \frac{1 - |g|^2}{12} \left(\frac{4\mu_1}{|\beta_1|(1 + |g|^2)} - \frac{1}{|g|} \right) \\ \frac{\eta^2}{|\beta_1|} &= \frac{1}{3} \left(\frac{8\mu_1}{|\beta_1|(1 + |g|^2)} + \frac{1}{|g|} \right). \end{aligned} \quad (5.25)$$

Figure 5.2 shows $|g|$ as a function of the flux for different values of the parameter $\mu_1/|\beta_1|$.

We see from this figure that there are two different regimes: for $\mu_1 < |\beta_1|/2$ (high temperature regime), $|g|$ is a single valued function of the flux, whereas for $\mu_1 > |\beta_1|/2$ there is a reentrance near $\phi \approx m + 1/2$. The fact that the transition between both regimes occurs at $\mu_1 = |\beta_1|/2$ can be verified by evaluating $d\phi_1/d|g|$ and $d^2\phi_1/d|g|^2$ and noting that both vanish at the same point $|g| = 1$. Therefore, there is a *critical point* at $(\phi = m + 1/2, \mu = 1/4 + \epsilon|\beta_1|/2)$ and we dub it P_2 . (The index “2” suggests that this is a second transition as the temperature is lowered; the first one is from normal to superconducting.)

Let us first discuss the case $\mu_1 < |\beta_1|/2$. The factor $(1 - |g|^2)$ ensures that $|g| = 1$ for $\phi_1 = 0$. This means that $e^{-mi\theta} + g e^{-(m+1)i\theta}$ in (5.22) vanishes for $\theta = \pi + \arg g$. We know already that $\beta_1 g$ is real. For $|g| = 1$ and $\phi_1 = 0$, (5.24) gives $\beta_1 g = -4\mu_1 + 3\eta^2$, which is positive at the onset of superconductivity and, by continuity, has to remain positive along the line $\phi_1 = 0$ in the entire high temperature regime. It follows that the leading term of ψ vanishes at $\theta = \pi - \arg \beta_1$. If the shape of $w(\theta)$ is dominated by the first harmonic, this means that the leading term of ψ vanishes at the thinnest part of the loop.

We are still left with the question of whether the entire order parameter vanishes at some point or whether the small contribution $\epsilon^{3/2}\psi_1$ remains. In [6] it is shown that the entire ψ vanishes at $\phi_1 = 0$. This can also be seen from

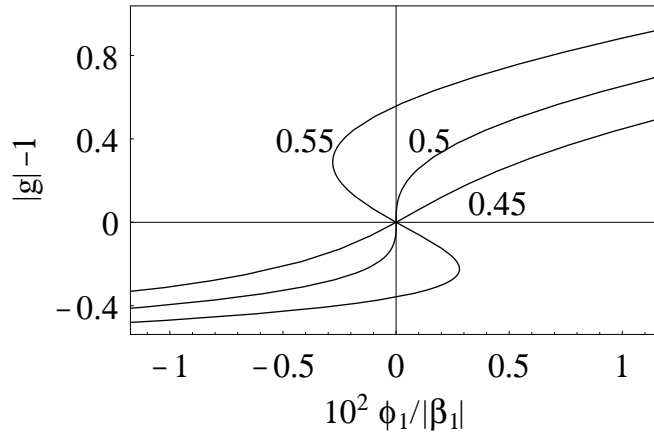


Figure 5.2. g determines the shape of the order parameter in Eq. (5.22); ϕ_1 measures the deviation of the flux from $(m + 1/2)\Phi_0$. Each curve is marked by its value of $\mu_1/|\beta_1|$. The curve $\mu_1/|\beta_1| = 1/2$ has infinite slope at $\phi_1 = 0$, indicating the presence of a critical point

continuity arguments: for $|g|$ appreciably smaller than 1, the winding number of ψ is m , whereas for $|g|$ appreciably greater than 1, its winding number is $m + 1$. Since ψ changes continuously with $|g|$, whereas its winding number does not, there must be some $|g|$ for which the winding number is undefined.

Note the qualitative difference between the cases of uniform and nonuniform cross section: in the first case, ψ is either proportional to $e^{-mi\theta}$ or to $e^{-(m+1)i\theta}$, and it is impossible to pass continuously from some m to the next; in the case of nonuniform cross section, ψ is a sum over all harmonics, with a higher weight at some m . As the flux increases and crosses $m + 1/2$, this weight is gradually transferred to $m + 1$ by increasing $|g|$ from $|g| \ll 1$ to $|g| \gg 1$.

Let us now consider the case $\mu_1 > |\beta_1|/2$. In this case there is a region (which for $\mu_1 \approx |\beta_1|/2$ is $|\phi_1| \lesssim 4|\beta_1|[\mu_1/(3|\beta_1|) - 1/6]^{3/2}$) where (5.25) has three solutions. At each extreme of this region, two solutions of the Euler-Lagrange equations coalesce, implying that the second variation of the free energy vanishes. This suggests that at these points the solution found becomes unstable. It is natural to conclude that the portion of Fig. 5.2 with negative slope, which is the continuation of the “bridging solution” of Section 5.3.1, is the unstable one. It follows that for $\mu_1 > |\beta_1|/2$ the order parameter will “jump” from winding number m to $m + 1$ as the flux is suitably increased, without going through a stable solution that breaks connectivity.

One of the most easily measurable quantities is the current I . Using (5.25) we obtain that, to leading order in ϵ , it is proportional to $(|g|^2 - 1)(1 + |g|^2 + 8|g|\mu_1/|\beta_1|)/(|g| + |g|^3)$. A usual experimental technique measures the a.c. susceptibility χ , which is proportional to $dI/d\phi$. It follows that χ is proportional to

$d|g|/d\phi_1$ and, therefore, diverges linearly at the stability limits and quadratically at the critical point P_2 . For experimental implications see [5].

Equations (5.24) are obtained by considering the m th and $(m+1)$ th harmonics in (5.21). The other harmonics give the leading terms of ψ_1 in (5.22), except for the harmonics m and $m+1$; in order to obtain these, perturbation to order $O(\epsilon^2)$ is required.

The reason that only β_1 appears in (5.24) is that only $e^{i\theta}$ can link between $e^{-mi\theta}$ and $e^{-(m+1)i\theta}$ in first order perturbation; in second order, the linkage could be made by any term of the form $\beta_{j+1}\beta_{-j}e^{i\theta}$. However, if the shape of $w(\theta)$ has an n -fold axis, so that all the harmonics of $w(\theta)$ are multiples of n , $e^{-mi\theta}$ and $e^{-(m+1)i\theta}$ cannot be linked in any order of perturbation. We may expect this to be related to a failure of assumption (3.10) when $w(\theta)$ has n -fold symmetry and the flux is half-integer.

5.4 Rings with Finite Width

In the previous sections we assumed that the “radial” dimension of the sample was very small compared to the coherence length ξ . In that case ψ depended only on the arc length and the problem became one-dimensional. In this section we release this assumption. One of the questions we want to answer is whether the zero which we found in previous sections when the flux is an integer plus half still breaks connectivity. Explicitly, does ψ now vanish on an entire surface that connects the inner and outer boundary, or only at a line parallel to the magnetic field, as in the case of vortices? We also want to find out whether the critical point P_2 of Section 5.3.2 and the singularities associated with it still exist, or whether these are smeared by the finite width of the shell.

In the zeroth order approximation we consider a cylindrical shell with inner radius R_i , outer radius $R_o = R_i + w$ and height h . In the typical situation we shall consider a uniform applied field $H_e\hat{z}$, where z is the axis of the shell.

For a thick shell the definition of the “enclosed” flux requires some convention, since the flux through the sample itself is not negligible. We shall adopt some conventions in the following subsections and in general define $\phi(r) = \pi H_e r^2 / \Phi_0$, the flux through a circle of radius r , in quantum units.

If the order parameter is small, the GL equation (5.2) becomes a linear separable equation, and was solved in Section 4.1.5. (See also [2].) The Neuman boundary conditions allow for lowest energy solutions that are independent of z , so that we are left with a two-dimensional problem which is independent of the height h of the sample. Writing the order parameter in the form

$$\psi_0^{(m)} = \mathcal{R}_m(r)e^{-mi\theta} \quad (5.26)$$

and choosing the gauge such that $\mathbf{A} = A(r)\hat{\theta}$, where θ is the angular cylindrical coordinate, the linearized GL equation becomes

$$-\mathcal{R}_m'' - \frac{\mathcal{R}_m'}{r} + \left(\frac{m}{r} - \tilde{A}\right)^2 \mathcal{R}_m = \mu \mathcal{R}_m, \quad (5.27)$$

where we have switched back to the dimensional notation $\mu = \xi^{-2}$. This has the solution

$$\mathcal{R}_m(r) = r^{|m|} e^{\phi(r)/2} [k_M M(\alpha, |m| + 1, \phi(r)) + k_U U(\alpha, |m| + 1, \phi(r))], \quad (5.28)$$

where M and U are Kummer's confluent hypergeometric functions, $\alpha = \frac{1}{2}(1 + |m| - m - \frac{1}{2}\mu_0/b)$, μ_0 (which depends on m and H_e) is the lowest eigenvalue for μ and $b = \pi H_e / \Phi_0$. The boundary conditions require that the derivative of $\mathcal{R}_m(r)$ vanish; these conditions can be written as $a_M k_M + a_U k_U = 0$ with

$$\begin{aligned} a_M &= 2(|m| + 1 - \alpha)M(\alpha - 1, |m| + 1, \phi(r)) \\ &\quad + (2\alpha + \phi(r) - 2 - |m|)M(\alpha, |m| + 1, \phi(r)) \\ a_U &= -2U(\alpha - 1, |m| + 1, \phi(r)) + (2\alpha + \phi(r) - 2 - |m|)U(\alpha, |m| + 1, \phi(r)) \end{aligned} \quad (5.29)$$

at $r = R_i$ and $r = R_o$. The constants k_M, k_U and the eigenvalue μ_0 are determined by three equations: $a_M k_M + a_U k_U = 0$ at $r = R_i$ or $r = R_o$, the determinant $a_M(R_i)a_U(R_o) - a_M(R_o)a_U(R_i)$ has to vanish, and some normalization (with suitable units) can be chosen. The winding number m has to be chosen so that the lowest value of μ_0 is obtained. It should be born in mind that these values are obtained from a system of nonlinear equations that has several solutions; we have made an effort to always pick the relevant solution, but the possibility of convergence to some other solution cannot be discarded.

A well known feature of the solution (5.28) is that there exist magnetic fields for which the linearized GL equation is degenerate. In the limit of a thin shell this occurs when the enclosed flux equals $(m + 1/2)\Phi_0$: for each of these fluxes, the eigenvalues μ_0 obtained for m and for $m + 1$ are the same and the lowest possible. If the shell is not thin, there still exist fluxes where the values of μ_0 for $\psi_0^{(m)} = \mathcal{R}_m(r) \exp(-mi\theta)$ and for $\psi_0^{(m+1)} = \mathcal{R}_{m+1}(r) \exp(-[m + 1]i\theta)$ coalesce, and we denote them by $\Phi_*^{(m)}$. As the magnetic field is swept across these fluxes, the equilibrium order parameter, and measurable quantities such as the current around the shell, change discontinuously.

5.4.1 Order of the Normal–Superconducting Transition

The opening of Section 5.4 describes the minimizer of the linearized GL potential, with the implicit assumption that the magnetic field is the same as the applied field. Linearization of this potential is a good approximation only if the order parameter is small. A natural question is whether there exists a situation where $|\psi|$ is small. This situation will occur at a bifurcation from the normal state, i.e. at a second order phase transition. In the following, we shall check the stability of the solution described above, namely, whether it is a local minimum of the entire GL potential.

The GL potential is a functional of two fields, ψ and \mathbf{A} , but we can first minimize w.r.t. \mathbf{A} and obtain

$$\nabla \times \nabla \times \tilde{\mathbf{A}}_i = \mathbf{J}, \quad (5.30a)$$

$$\mathbf{J} = \frac{\mu}{\kappa^2} \text{Re}[\bar{\psi}(i\nabla - \tilde{\mathbf{A}})\psi], \quad (5.30b)$$

where we have separated $\tilde{\mathbf{A}}$ into an external part $\tilde{\mathbf{A}}_e$, due to the applied field, and an induced part $\tilde{\mathbf{A}}_i$, due to the supercurrents, which vanishes far from the sample; (5.30a) is Ampère's law and \mathbf{J} is the supercurrent density. (In Gaussian units, the current density is $c\Phi_0\mathbf{J}/[2(2\pi)^2]$.) From here we learn that, for small $|\psi|$, $\tilde{\mathbf{A}}_i$ is quadratic in ψ , decreases with κ^2 and, if the current has to circulate through some cross section, we expect $\tilde{\mathbf{A}}_i$ to be an increasing function of it.

The form (5.1) of the GL potential guarantees that the order parameter of the minimizer is bounded. Moreover, it has been shown [14] that $|\psi|$ is always bounded by 1. Having in mind a small $|\psi|$, we denote by \mathbf{J}_2 the value of \mathbf{J} which is obtained by replacing $\tilde{\mathbf{A}}$ with $\tilde{\mathbf{A}}_e$ in (5.30b), and then expand $\tilde{\mathbf{A}}_i = \tilde{\mathbf{A}}_{i2} + \tilde{\mathbf{A}}_+$, where $\nabla \times \nabla \times \tilde{\mathbf{A}}_{i2} = \mathbf{J}_2$ and $\tilde{\mathbf{A}}_+$ fulfills

$$\nabla \times \nabla \times \tilde{\mathbf{A}}_+ = -(\mu/\kappa^2)|\psi|^2(\tilde{\mathbf{A}}_+ + \tilde{\mathbf{A}}_{i2}). \quad (5.31)$$

For the cylindrical shells considered above, it is easy to evaluate $\tilde{\mathbf{A}}_{i2}$ in the limits $h \gg R_o$ and $h \ll \kappa\xi$. In the first case we have a two dimensional problem and, using cylindrical symmetry and writing $\tilde{\mathbf{A}}_{i2} = \tilde{A}_{i2}(r)\hat{\theta}$, we are left with an ordinary differential equation for \tilde{A}_{i2} , which can be solved numerically. The boundary conditions are $\nabla \times \tilde{\mathbf{A}}_{i2} = 0$ at R_o , which gives $\tilde{A}'_{i2}(R_o) = -\tilde{A}_{i2}(R_o)/R_o$, and continuity of $\tilde{\mathbf{A}}_{i2}$ at $r = 0$ together with continuity of $\nabla \times \tilde{\mathbf{A}}_{i2}$ at R_i , which require $\tilde{A}'_{i2}(R_i) = \tilde{A}_{i2}(R_i)/R_i$. In the three dimensional problem, $\tilde{\mathbf{A}}_{i2}(\mathbf{r})$ can be evaluated by integrating the Green's function $\mathbf{J}_2(\mathbf{r}')/(4\pi|\mathbf{r} - \mathbf{r}'|)$. For $h \ll \kappa\xi$, \mathbf{r} and \mathbf{r}' are required only on the same plane; in this case we can perform the integration over θ' analytically and are left with a numeric integration over r' . The integrand has a singularity at $r' = r$, which has to be treated separately.

Let us now regard $\tilde{\mathbf{A}}_i$ and \mathbf{J} as known functions of ψ . Noting that $|\nabla \times \tilde{\mathbf{A}}_i|^2 = \nabla \cdot (\tilde{\mathbf{A}}_i \times (\nabla \times \tilde{\mathbf{A}}_i)) + \tilde{\mathbf{A}}_i \cdot (\nabla \times \nabla \times \tilde{\mathbf{A}}_i)$, using (5.30a) and (5.30b) and the fact that \tilde{A}_i decays sufficiently fast far from the sample, the GL potential can be written in the form

$$G = G_2 + G_4 + G_+ \quad (5.32)$$

with

$$\begin{aligned} G_2 &= \int \left(-\mu|\psi|^2 + \left| (i\nabla - \tilde{\mathbf{A}}_e) \psi \right|^2 \right) \\ G_4 &= \mu \int \left(\frac{1}{2}|\psi|^4 - \kappa^{-2} \frac{\kappa^2 \tilde{\mathbf{A}}_{i2}}{\mu} \cdot \frac{\kappa^2 \mathbf{J}_2}{\mu} \right) \\ G_+ &= -\frac{\kappa^2}{\mu} \int \tilde{\mathbf{A}}_+ \cdot \mathbf{J}_2, \end{aligned} \quad (5.33)$$

where the integrals are over the sample. Following (5.30a) and (5.30b), μ and κ have been factored out in the expression for G_4 . G_n depends on the shape of ψ and is proportional to the n th power of the "size of ψ ".

In the linearized GL formalism, G is replaced by G_2 . Clearly, for small μ and $\tilde{\mathbf{A}}_e \neq 0$, $G_2 \geq 0$ and the minimizer is the normal state $\psi = 0$. As μ increases,

there are two possibilities: if $G_4 > 0$, then, for μ such that $G_2 < 0$, G_2 will dominate for small sizes of ψ , forcing a bifurcation from $\psi = 0$, but for large sizes, G_4 will dominate, keeping ψ at a limited size; this size increases continuously with μ from $\psi = 0$, so that the transition is of second order. On the other hand, if $G_4 < 0$ for some shape of ψ , it may pay to pass over to this ψ even before G_2 becomes negative. However, the positive G_2 will act as a potential barrier and prevent ψ from leaving the normal state, unless it is sufficiently large. Therefore, there will be a discontinuous (first order) transition, and the size of ψ will be limited by G_+ .

It follows that the order of the transition depends on the sign of G_4 . For a wide range of parameters, we always found $\int \mathbf{A}_{i2} \cdot \mathbf{J}_2 > 0$. (\mathbf{A}_i tends to be in the same direction as the current that generates it.) Therefore, the transition from normal to superconducting state will be of first order if κ is sufficiently small and of second order if κ is sufficiently large. We shall denote by κ_c the limiting value between both regimes. The expression for G_4 suggests that κ_c will be larger under conditions that yield larger currents: larger cross section, more connectivity, magnetic fluxes which are not integer.

Figures 5.3(a)–(c) show lower bounds for κ_c as functions of the ratio $(R_o - R_i)/R_o$ between the width of the shell and its outer radius, for the case $h \gg R_o$. These were evaluated by using the shape of ψ that minimizes G_2 , i.e. (5.28), to check the sign of G_4 . G_4 must be positive for a second order transition, since otherwise the order parameter predicted by assuming a second order transition would not be stable. κ_c has been calculated for different values of the winding number and the flux. In order to have a “fair comparison” of the “enclosed” fluxes among shells that differ in width, we define the “adjusted flux” ϕ_{ad} as follows: in the absence of magnetic field, $\phi_{\text{ad}} = 0$; at $\Phi_*^{(m)}$ ($m \geq 0$), $\phi_{\text{ad}} = m + 1/2$; between these values, ϕ_{ad} is a linear function of the flux. In the limit of a thin shell ($R_i \approx R_o$), ϕ_{ad} is just the flux in units of Φ_0 .

For thin shells, the current density is proportional to $\phi_{\text{ad}} - m$, the induced potential to $(\phi_{\text{ad}} - m)w$, and κ_c^2 , to $(\phi_{\text{ad}} - m)^2 w$. For an almost full cylinder, a situation with $m < \phi_{\text{ad}}$ has higher κ_c than a similar situation with $m > \phi_{\text{ad}}$; this may reflect the fact that a larger winding number shrinks the width of the region where currents circulate and also favors competition between paramagnetic and diamagnetic currents. κ_c does not increase monotonically with the width, but has a peak; for a given ϕ_{ad} , this peak is located roughly at the width for which $\phi(R_o)$ is maximum. The height of this peak remains nearly constant at about $\sqrt{1/2}$, the known limit between superconductivities of types I and II; we have no intuitive explanation for this result. For large fluxes, κ_c becomes independent of the width shortly beyond the peak. The reason for this is that superconductivity is appreciable only close to the outer boundary, so that the inner part of the shell becomes irrelevant.

Figure 5.3(d) shows κ_c for the case $h \ll \kappa\xi$. The results are qualitatively the same as for the long shells, but κ_c^2 has to be scaled by $h\sqrt{\mu}$.

We already know when the normal-superconducting transition must be discontinuous. It would be interesting to have at least an estimate for the value of κ

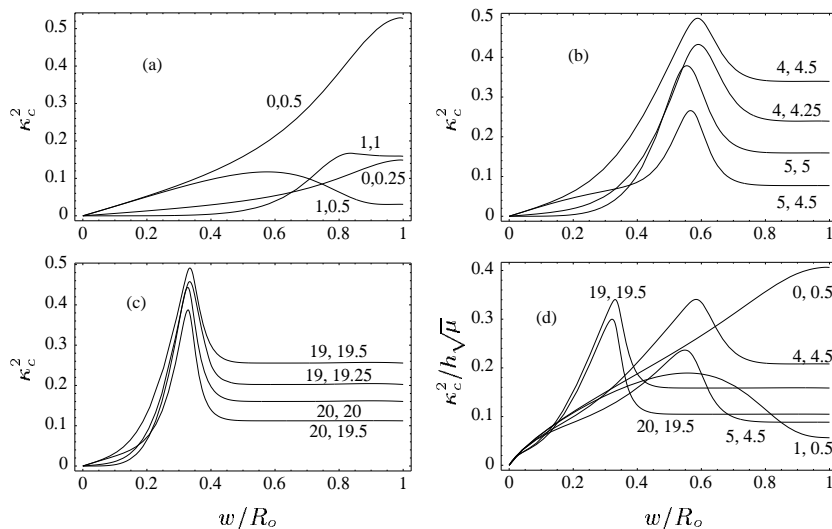


Figure 5.3. Lower bounds for κ_c as functions of the width of the shell. Below these lines, the normal/superconducting transition is of first order. Each line is marked with two numbers: the first is the winding number and the second, the “adjusted flux” ϕ_{ad} . (a)–(c): long shells; (d): flat rings

for which it *could* be discontinuous. It is tempting to argue that such an estimate could be obtained by evaluating G_4 for the shape of ψ that minimizes G_4 itself, rather than G_2 . However, this criterion gives very poor estimates, especially for high fluxes and large ratio $(R_o - R_i)/R_o$.

Figure 5.4 shows the GL potential G as a function of the size of the order parameter, for several values of the temperature, for a long full sample ($h \gg R_o$, $R_i = 0$). In the figure, the “size” has been defined as the average of $|\psi|^2$, $\int |\psi|^2 r dr / \int r dr$, and the shape of ψ has been taken so as to minimize G for the chosen size. Unlike the case of Figs. 5.3, the shape of ψ minimizes the entire potential, and not only G_2 . In the calculations we have made two assumptions: first, we assume that ψ has the symmetry of the problem, i.e. is a radial function times $e^{-mi\theta}$ and, second, we have kept in G only the contributions up to $O(|\psi|^6)$, i.e. we dropped $\tilde{\mathbf{A}}_+$ at the r.h.s. of (5.31). For the values of the flux considered [$\phi(R_o) = 2.1$], the best candidates for a minimum of G are $m = 0$ and $m = 1$.

For high temperature ($\mu R_o^2 = 1.7$), both curves have their minima at $\psi \equiv 0$, so that the sample has to be in the normal state. As the temperature is lowered to $\mu R_o^2 = 1.8$, G could be lowered if the sample had an order parameter with winding number 0 and size of about 0.15. In order to pass from the normal to this new state, ψ would have to “jump”, so that the normal state is still a local minimum. When the temperature is lowered to $\mu R_o^2 = 1.9$, the normal state becomes unstable, not with respect to $m = 0$, but rather with respect to $m = 1$. In summary, the shape of the order parameter obtained when the sample is

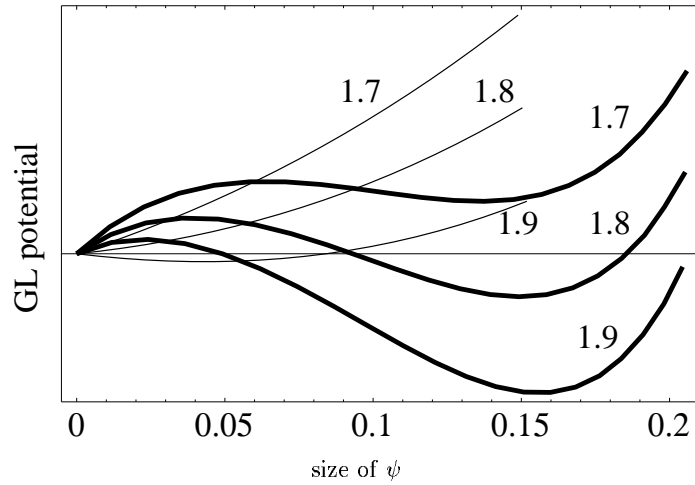


Figure 5.4. Superconducting energy of a cylinder as a function of the size of the order parameter, for fixed flux and various values of the temperature and the winding number. Here $\phi(R_o) = 2.1$ and $\kappa^2 = 0.1$; the lines are marked by the value of μR_o^2 . Thick lines: $m = 0$; thin lines: $m = 1$.

cooled from $\mu R_o^2 = 1.7$ to $\mu R_o^2 = 1.9$ depends on how it is cooled: if it is cooled carefully, so that the jump is avoided, we must obtain $m = 1$; if it is left for a long time at $\mu R_o^2 = 1.8$ and forced to jump, we must obtain $m = 0$.

Figure 5.4 is good as an illustration, but the assumptions that led to it are not necessarily justified. The sizes of ψ are small in the range considered, but μ/κ^2 is large, so that $G_{2(n+1)}$ is smaller than G_{2n} just by a moderate factor. Actually, if $G_4 < 0$ and G_6 were negligible, then G would not have a finite minimum. As for the second assumption, since the GL equations are nonlinear, the minimizer may not have the entire symmetry of the problem. It is known [3] that, for appropriate parameters in cylindrical samples, ψ would vanish along a single line that does not coalesce with the cylinder axis.

If h is of the same order of magnitude as R_o , one might expect to have an intermediate situation between the two extremes considered here. However, a complication appears: at the corners ($r = R_o, z = \pm h/2$) a very large demagnetizing field develops that forces these corners to remain normal [8].

In the following subsections we shall consider transitions of second order, so that we may deal with situations where expansions on powers of ψ can provide a good description. In view of Fig. 5.3(d), these are frequently encountered situations, since in many experiments $h\sqrt{\mu}$ is small.

5.4.2 Nonuniform Cross Section – Nondegenerate Perturbation

Our purpose now is to extend the treatment of Section 5.3.2 to rings of finite width. The main objective of this subsection will be to evaluate the temperature

for the onset of superconductivity. This temperature is a monotonic function of the eigenvalue μ of the linearized GL equation. We write

$$\begin{aligned}\mu &= \mu_0 + \epsilon\mu_1 + \epsilon^2\mu_2 + \dots, \\ \psi &= \psi_0 + \epsilon\psi_1 + \dots,\end{aligned}\tag{5.34}$$

where ψ_0 is given by (5.26) and (5.28) [we omit here the index (m)] and μ_0 is determined as described after (5.29). We now want to determine μ_1 and μ_2 . Introducing (5.34) into the linearized GL equation gives to first order in ϵ

$$(\mathcal{H}_0 - \mu_0)\psi_1 = \mu_1\psi_0,\tag{5.35}$$

where the operator \mathcal{H}_0 is now

$$\mathcal{H}_0 = \left(i\nabla - br\hat{\theta}\right)^2\tag{5.36}$$

and b was defined after (5.28).

Let us now define a metric by integrating in the *unperturbed* region:

$$(\phi_1, \phi_2) = \int_{-h/2}^{h/2} dz \int_0^{2\pi} d\theta \int_{R_i}^{R_o} r dr \bar{\phi}_1 \phi_2.\tag{5.37}$$

In the subspace of functions that have Neuman boundary conditions \mathcal{H}_0 is Hermitic, but in general, it has the property

$$(\phi_1, \mathcal{H}_0\phi_2) - (\mathcal{H}_0\phi_1, \phi_2) = \int_{\partial\Omega} (\phi_2\nabla\bar{\phi}_1 - \bar{\phi}_1\nabla\phi_2) \cdot \hat{\nu}_0,\tag{5.38}$$

where $\int_{\partial\Omega}$ denotes integration over the surface of the unperturbed sample and $\hat{\nu}_0$ is the unit vector normal to this surface. For example, if the only perturbation in the shape of the sample is in its outer boundary and, in addition, this perturbation is independent of z , (5.38) becomes

$$(\phi_1, \mathcal{H}_0\phi_2) - (\mathcal{H}_0\phi_1, \phi_2) = hR_o \int_0^{2\pi} \left(\phi_2 \frac{\partial\bar{\phi}_1}{\partial r} - \bar{\phi}_1 \frac{\partial\phi_2}{\partial r}\right) d\theta.\tag{5.39}$$

In the following, we shall consider only this situation: the inner boundary of the shell will be located at $r = R_i$ and the outer one at $r = R_i + w(\theta)$, where $w(\theta)$ is given by (5.20).

Projecting Eq. (5.35) onto ψ_0 and using (5.39) we obtain

$$\mu_1 = -\frac{hR_o}{(\psi_0, \psi_0)} \int_0^{2\pi} \bar{\psi}_0 \frac{\partial\psi_1}{\partial r} d\theta.$$

$\partial\psi_1/\partial r$ is obtained by requiring that the normal component of $(i\nabla - \tilde{\mathbf{A}})(\psi_0 + \epsilon\psi_1)$ vanish to order ϵ at the boundary $r = R_i + w(\theta)$. Expanding around $r = R_o$ gives

$$\frac{\partial\psi_1}{\partial r} = -\frac{w}{2} \sum_{j \neq 0} \beta_j e^{(j-m)i\theta} \left(\frac{d^2}{dr^2} + jb - \frac{jm}{r^2}\right) \mathcal{R}_m(r),\tag{5.40}$$

evaluated at $r = R_o$. We see that $\partial\psi_1/\partial r$ does not contain the $(-m)$ -th harmonic and therefore $\mu_1 = 0$. It follows that the differential equation (5.35) for ψ_1 is the same as the equation we had for ψ_0 , but the boundary condition has been modified. We write $\psi_1 = \sum_{l \neq m} \mathcal{Y}_l(r)e^{-il\theta}$. The solution of (5.35) for every harmonic is of the form (5.28), but at $r = R_o$ the Neuman condition has to be replaced by (5.40). We find

$$\mathcal{Y}_l(r) = \frac{1}{2} \frac{w\beta_{m-l}c_{l,m}\mathcal{R}_m(R_o)}{a_M(l; R_o)a_U(l; R_i) - a_M(l; R_i)a_U(l; R_o)} \left(\frac{r}{R_o}\right)^{|l|} e^{b(R_o^2-r^2)/2} \times \\ [a_U(l; R_i)M(\alpha, |l| + 1, br^2) - a_M(l; R_i)U(\alpha, |l| + 1, br^2)], \quad (5.41)$$

where $a_{M,U}(l; r)$ are the functions defined in (5.29), with l substituted into m , and $c_{l,m} = R_o[\mu_0 - (bR_o - l/R_o)(bR_o - m/R_o)]$. The second derivative which appears in (5.40) was eliminated using the differential equation for \mathcal{R}_m .

μ_2 is obtained by the same arguments that lead to μ_1 . We obtain

$$\mu_2 = -\frac{w\mathcal{R}_m(R_o)}{2B_m} \left\{ \sum_{l \neq m} \beta_{l-m}c_{l,m}\mathcal{Y}_l(R_o) + \right. \\ \left. \frac{w\mathcal{R}_m(R_o)}{4} \left[\mu_0 - (bR_o - \frac{m}{R_o})(3bR_o + \frac{m}{R_o}) \right] \sum_{j \neq 0} |\beta_j|^2 \right\}, \quad (5.42)$$

with

$$B_m = \int_{R_i}^{R_o} r\mathcal{R}_m^2 dr. \quad (5.43)$$

Note that \mathcal{R}_m depends on the applied field and so does B_m .

5.4.3 Degenerate Perturbation

At the degeneracy flux $\Phi_*^{(m)}$, the determinant $a_M(R_i)a_U(R_o) - a_M(R_o)a_U(R_i)$ vanishes simultaneously for the winding numbers m and $m + 1$. Thus, \mathcal{Y}_{m+1} in (5.41) diverges. To handle this problem we have to use degenerate perturbation theory.

An additional difference between this and the previous subsection is that now we will be interested in knowing the order parameter for some region beyond the onset of superconductivity; therefore, the nonlinear term in (5.2) is not entirely neglected. We shall nevertheless neglect the induced magnetic potential. We expect this to be justified when $\mu h w \kappa^{-2} \ll 1$, so that the current is small. Still, we shall consider the region where $|\mu - \mu_P^{(m)}|$ is at most of order ϵ , where $\mu_P^{(m)}$ is the value of μ_0 for $\Phi = \Phi_*^{(m)}$.

Let us set the convention that “the” flux Φ is that through the outer boundary and let us write $\Phi = \Phi_*^{(m)} + \epsilon\phi_1\Phi_0$. Then the magnetic potential will be $\tilde{\mathbf{A}} =$

$(b_m + \epsilon\phi_1/R_o^2)r\hat{\theta}$, with $b_m = \Phi_*^{(m)}/(R_o^2\Phi_0)$. We denote by \mathcal{H}_P the operator \mathcal{H}_0 in (5.36) with b substituted by b_m . For the order parameter we write

$$\psi = \sqrt{\eta\epsilon}(\psi_0^{(m)} + g\psi_0^{(m+1)} + \epsilon\psi_1 + \dots) \quad (5.44)$$

where η and g still have to be determined by the perturbation procedure. Introducing these expressions into (5.2) we obtain, to lowest order in ϵ ,

$$(\mathcal{H}_P - \mu_P^{(m)})\psi_1 = f_m(r)e^{-mi\theta} + gg_m(r)e^{-(m+1)i\theta} + \eta \times (\text{other harmonics}) \quad (5.45)$$

with

$$\begin{aligned} f_m &= [2(\phi_1/R_o^2)(m - b_m r^2) + (\mu - \mu_P^{(m)})/\epsilon - \eta\mu_P^{(m)}(\mathcal{R}_m^2 + 2g^2\mathcal{R}_{m+1}^2)]\mathcal{R}_m, \\ g_m &= [2(\phi_1/R_o^2)(m + 1 - b_m r^2) + (\mu - \mu_P^{(m)})/\epsilon - \eta\mu_P^{(m)}(2\mathcal{R}_m^2 + g^2\mathcal{R}_{m+1}^2)]\mathcal{R}_{m+1}. \end{aligned} \quad (5.46)$$

We project this expression onto $\psi_0^{(m)}$ and use (5.39), and then repeat this procedure for $\psi_0^{(m+1)}$. This leads to a system of equations for g and η :

$$\begin{aligned} A_m\phi_1 + B_m(\mu - \mu_P^{(m)})/\epsilon &= (Q_m + g^2S_m)\eta - C_m\beta_1g, \\ A'_{m+1}\phi_1 + B'_{m+1}(\mu - \mu_P^{(m)})/\epsilon &= (g^2Q'_{m+1} + S_m)\eta - C_m\bar{\beta}_1/g, \end{aligned} \quad (5.47)$$

where B_m was defined in (5.43) and

$$A_m = 2R_o^{-2} \int_{R_i}^{R_o} (mr - b_m r^3)\mathcal{R}_m^2 dr, \quad (5.48a)$$

$$C_m = \frac{w}{2}c_{m+1,m}\mathcal{R}_m(R_o)\mathcal{R}_{m+1}(R_o), \quad (5.48b)$$

$$Q_m = \mu_P^{(m)} \int_{R_i}^{R_o} r\mathcal{R}_m^4 dr, \quad (5.48c)$$

$$S_m = 2\mu_P^{(m)} \int_{R_i}^{R_o} r\mathcal{R}_m^2\mathcal{R}_{m+1}^2. \quad (5.48d)$$

The primes in the second equation in (5.47) mean that b_m and $\mu_P^{(m)}$ are kept unchanged when the index m is substituted by $m+1$. Likewise, $c_{m+1,m}$ [defined after (5.41)] is evaluated at $b = b_m$. Note that the coefficients A_m , A'_m , B_m , B'_m , Q_m , Q'_m and S_m do not depend on the deviation of the shape of the sample from perfect axial symmetry. Eq. (5.48b) was obtained for a deviation at the outer boundary which depends only on θ ; in the general case, $C_m\beta_1$ has to be replaced by

$$\frac{1}{h} \int_{\partial\Omega} \left[\psi_0^{(m+1)} \mu_P^{(m)} \overline{\psi_0^{(m)}} - (i\nabla - \tilde{\mathbf{A}})\psi_0^{(m+1)} \cdot \overline{(i\nabla - \tilde{\mathbf{A}})\psi_0^{(m)}} \right] \nu, \quad (5.49)$$

where $\epsilon\nu$ denotes how far out one has to move from the unperturbed sample (in the direction normal to it) until the corresponding point in the boundary of the perturbed sample is reached.

The values of these coefficients depend on the normalizations of $\psi_0^{(m)}$ and $\psi_0^{(m+1)}$; accordingly, this affects the values of η and g so that the order parameter itself and the transition temperature are independent of the normalizations. As a final observation, we note that $g\beta_1$ has to be real. The phase of β_1 depends on the origin of the axial angle θ and we choose it such that $\beta_1 < 0$. If $w(\theta)$ is symmetric about $\theta = 0$ and $\theta = \pi$ and monotonic for $0 \leq \theta \leq \pi$, this choice means that the shell is thinnest at $\theta = 0$. It follows that g will be real.

In the remainder of this subsection, we push the perturbation procedure further for the onset of superconductivity, where $\eta = 0$. The line for the onset of superconductivity in the temperature - magnetic flux plane will be denoted by Γ_1 . We write $\mu = \mu_P^{(m)} + \epsilon\mu_1 + \epsilon^2\mu_2 + \dots$ (Unlike μ_0 , $\mu_P^{(m)}$ does not vary with the flux.) The first order correction μ_1 is obtained by solving (5.47). There are two solutions and we choose the lowest:

$$\mu_1 = -\frac{1}{2} \left[\left(\frac{A_m}{B_m} + \frac{A'_{m+1}}{B'_{m+1}} \right) \phi_1 + \sqrt{\frac{(2C_m\beta_1)^2}{B_m B'_{m+1}} + \left(\frac{A_m}{B_m} - \frac{A'_{m+1}}{B'_{m+1}} \right)^2 \phi_1^2} \right]. \quad (5.50)$$

From here and (5.47) it follows that $C_m\beta_1g/B_m = -\mu_1 - (A_m/B_m)\phi_1$ is always positive and, since $B_m > 0$ and $\beta_1 < 0$,

$$C_m g < 0 \quad (5.51)$$

along the transition line Γ_1 and close to $\Phi_*^{(m)}$. By continuity, and since we expect g to depend mainly on the flux and only marginally on the temperature, this inequality is expected to hold in the entire region of order ϵ investigated here.

For every l different from either m or $m+1$, \mathcal{Y}_l obeys the same differential equation as for the unperturbed case. However, now the leading term in (5.44) contains two contributions. Both contributions will be present in $\partial\psi_1/\partial r$, which appears in the boundary conditions for \mathcal{Y}_l , and therefore Eq. (5.41) is modified and contains a second term. The case of l equal to either m or $m+1$ requires special treatment. We describe here the case $l = m$; $l = m+1$ is entirely analogous.

\mathcal{Y}_m satisfies the inhomogeneous equation

$$\mathcal{Y}_m'' + \frac{1}{r}\mathcal{Y}_m' + \left[\mu_P^{(m)} - \left(b_m r - \frac{m}{r} \right)^2 \right] \mathcal{Y}_m = -f_m, \quad (5.52)$$

where $(\mu - \mu_P^{(m)})/\epsilon$ is replaced by μ_1 and η by 0. This is subject to the conditions that \mathcal{Y}_m' vanishes at $r = R_i$ and leads to the appropriate value of $\partial\psi_1/\partial r$ at $r = R_o$. Since μ_1 has been picked as an eigenvalue, if one of these conditions is fulfilled, the second follows automatically. One solution of (5.52) with the appropriate boundary conditions, which we denote by $y_m(r)$, can be obtained by solving (5.52) numerically, with $y_m(0) = y_m'(0) = 0$. This is not the only solution: any function $\mathcal{Y}_m(r) = y_m(r) + K_m \mathcal{R}_m(r)$ will be a solution, too.

We proceed now to second order perturbation (at the onset of superconductivity). We obtain $(\mathcal{H}_P - \mu_P^{(m)})\psi_2 = (\mu_2 - \phi_1^2 r^2/R_o^4)\psi_0 + \mu_1\psi_1$, with $\psi_0 =$

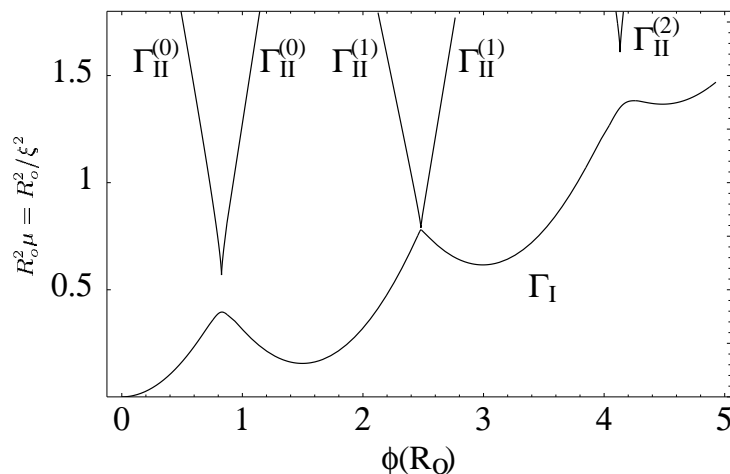


Figure 5.5. Phase diagram in the temperature - magnetic flux plane ($\mu \propto T_c - T$). The sample is normal below the line Γ_I and superconducting above it. At the left branch of $\Gamma_{II}^{(m)}$, the state with winding number $m + 1$ becomes unstable and must decay into m ; at its right branch, m decays into $m + 1$. The points $P_1^{(m)}$ are the maxima of Γ_I and $P_2^{(m)}$ are the minima of Γ_{II} . For the evaluation of this phase diagram we have used $w/R_o = 0.426$ (as in Refs. [17,18]), $\epsilon|\beta_1| = 0.15$ and $\beta_i = 0$ for $i > 1$. Γ_I was evaluated to $O(\epsilon^2)$ and Γ_{II} , to $O(\epsilon)$. For this ratio w/R_o , C_1 is small, so that Γ_I and $\Gamma_{II}^{(1)}$ almost touch

$\psi_0^{(m)} + g\psi_0^{(m+1)}$. Projecting onto $\psi_0^{(m)}$ and $\psi_0^{(m+1)}$, using (5.39) and keeping terms up to $O(\epsilon^2)$ leads to two equations for μ_2 , K_m and K_{m+1} . The third equation is provided by some normalization criterion, which is usually taken as $(\psi_1, \psi_0) = 0$. From here, μ_2 and the missing information for ψ_1 are obtained.

The onset for superconductivity occurs at the lowest line in Fig. 5.5 (Γ_I). This line was obtained by seven different algorithms: near $\Phi = \Phi_*^{(m)}$ ($m = 0, 1, 2$) we used degenerate perturbation; far from $\Phi = \Phi_*^{(m)}$ we used (5.42).

5.4.4 Critical Points

In Section 5.3.2 we found that thin loops have two critical points in the temperature - magnetic flux diagram, which we denote by P_1 and P_2 . Here we extend this result to shells which are not necessarily thin.

$P_1^{(m)}$ is defined as the point on the critical line Γ_I such that the sample always remains superconducting as the field is swept close to $\Phi = \Phi_*^{(m)}$ for temperatures below that of $P_1^{(m)}$, whereas it passes through the normal state if the temperature is higher than that of $P_1^{(m)}$. (See Fig. 5.5.) $P_2^{(m)}$ is defined as the point on a critical line $\Gamma_{II}^{(m)}$ such that, for temperatures below that of $P_2^{(m)}$, there is a first order transition when the field is swept close to $\Phi = \Phi_*^{(m)}$, whereas the order

parameter changes smoothly if the temperature is higher than that of $P_2^{(m)}$. The analysis of this subsection will be kept to first order in ϵ .

$P_1^{(m)}$ is obtained by maximizing (5.50). This gives

$$\begin{aligned}\phi_1 &= \frac{A_m B'_{m+1} + A'_{m+1} B_m}{A_m B'_{m+1} - A'_{m+1} B_m} \frac{|C_m \beta_1|}{\sqrt{-A_m A'_{m+1}}} \\ \mu_1 &= \frac{2|C_m \beta_1| \sqrt{-A_m A'_{m+1}}}{A_m B'_{m+1} - A'_{m+1} B_m}.\end{aligned}\quad (5.53)$$

If w/R_o is sufficiently small, $A_m < 0$ and $A'_{m+1} > 0$. However, as w/R_o increases, A'_{m+1} eventually becomes negative and the temperature for the onset of superconductivity becomes a monotonic function of the flux close to $\Phi = \Phi_*^{(m)}$. The middle column of Table 5.1 shows the values of w/R_o for which A'_{m+1} vanishes. Generically, I_1 has cusplike maxima for low fluxes and rises monotonically for high fluxes; for a full (or nearly full) disk, I_1 is monotonic in the entire range, and for a very thin shell, I_1 has maxima up to very high fluxes.

Table 5.1. Values of the width/radius ratio, w/R_o , for which A'_{m+1} or C_m vanishes. If w/R_o is smaller than the value for which $A'_{m+1} = 0$, then the transition value of μ has a local maximum near $\Phi = \Phi_*^{(m)}$; if w/R_o is smaller than the value for which $C_m = 0$, then vortices pass through the thin part of the sample.

m	$A'_{m+1} = 0$	$C_m = 0$
0	0.8673	1.0000
1	0.6137	0.4436
2	0.5138	0.2940
3	0.4537	0.2197
4	0.4119	0.1753
5	0.3806	0.1458
6	0.3558	0.1248
7	0.3356	0.1091
8	0.3187	0.0969
9	0.3042	0.0872
10	0.2916	0.0792

For given values of $(\mu - \mu_P^{(m)})$ and ϕ_1 , η and g can be obtained from equations (5.47). Figure 5.6 shows $|g|$ as a function of the flux for different values of the parameter $(\mu - \mu_P^{(m)})$. Qualitatively, we recover the behavior of Fig. 5.2. We see that, for $(\mu - \mu_P^{(m)})$ sufficiently large, there is an unstable branch; when

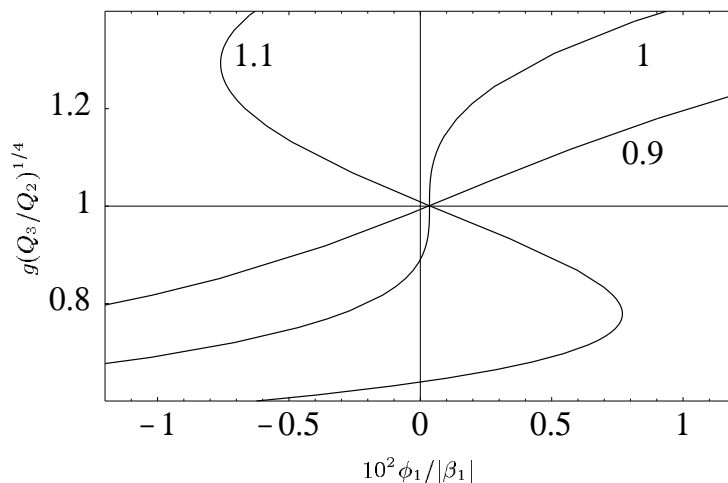


Figure 5.6. $|g|$ as a function of the flux, for several values of the coherence length. (Q_m and $Q'_{(m+1)}$ provide a normalization constant.) For each curve, $(\mu - \mu_P^{(m)})/\epsilon$ equals the value of μ_1 given in (5.54), times the number shown next to the curve. The behavior is the same as in the case of an infinitesimally thin shell. For the evaluation of these curves we have used $w/R_o = 0.426$ and $m = 2$. (For these values, $g > 0$.)

it is reached as the flux is swept, g jumps to the other stable branch. The stability limit is characterized by $d\phi_1/dg = 0$, and its locus in the temperature - flux diagram is the curve $\Gamma_{\text{II}}^{(m)}$ in Fig. 5.5. The lowest point in this curve, $P_2^{(m)}$, is obtained by requiring in addition $d^2\phi_1/dg^2 = 0$. At this point we find $|g| = (Q_m/Q'_{m+1})^{1/4}$,

$$\mu_1 = \frac{2|C_m|\beta_1(Q_m Q'_{m+1})^{1/4}(A_m \sqrt{Q'_{m+1}} - A'_{m+1} \sqrt{Q_m})}{(A_m B_{m+1} - A'_{m+1} B_m)(\sqrt{Q_m Q'_{m+1}} - S_m)}, \quad (5.54)$$

and $\phi_1 = -\mu_1(B_m \sqrt{Q'_{m+1}} - B_{m+1} \sqrt{Q_m})/(A_m \sqrt{Q'_{m+1}} - A'_{m+1} \sqrt{Q_m})$. Figure 5.7 shows the temperatures of $P_1^{(m)}$ and $P_2^{(m)}$, as functions of the width of the shell, for small values of m .

Most experiments are performed at constant temperature, while the magnetic field is varied, i.e., along a horizontal line in Fig. 5.5. The experimental response will be a continuous function of the flux if the temperature is between those of $P_1^{(m)}$ and $P_2^{(m)}$, but will exhibit hysteresis if the temperature is below that of $P_2^{(m)}$.

Figure 5.5 suggests that discontinuous transitions will usually be encountered for low fluxes, whereas close to Γ_1 continuous behavior prevails. However, anomalous behavior is also possible: the temperature of $P_2^{(m)}$ usually decreases with m , because $\mu_P^{(m)}$ increases with m ; on the other hand, μ_1 in (5.54) is not a monotonic function of m , and usually has a minimum near the value of m

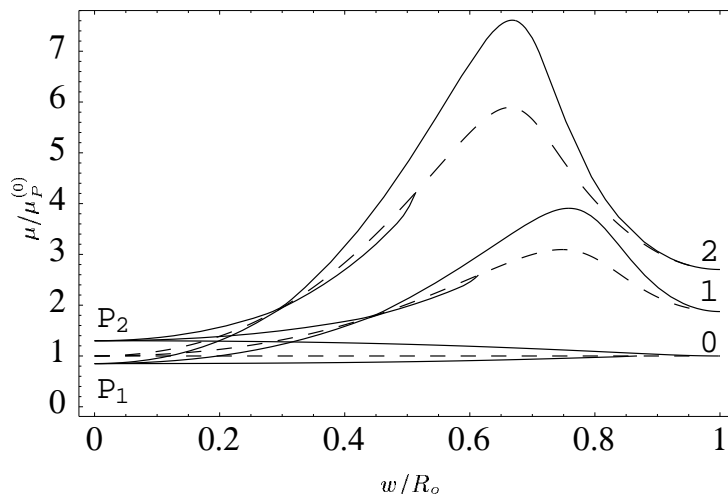


Figure 5.7. Comparison among the values of $\mu = \xi^{-2}$ at the critical points, as functions of the width w of the sample. The dashed lines describe $\mu_P^{(m)}$; the values of μ for P_1 and P_2 are below and above each of them. The winding numbers m are shown at the right. The distances between the values of μ at $P_{1,2}^{(m)}$ and $\mu_P^{(m)}$ are proportional to $\epsilon|\beta_1|$, which is taken here as 0.15. They are also proportional to C_m , and therefore the three lines touch each other when $C_m = 0$; this happens at the value of w/R_o given in Table 5.1, and again at $w = R_o$. When $A'_{m+1} = 0$, the line for $P_1^{(m)}$ collapses into that of $\mu_P^{(m)}$. For $w \ll R_o$, $P_{1,2}$ and μ_P become independent of m .

where C_m changes sign. It follows that, for sufficiently large values of $\epsilon|\beta_1|$, the temperature for some $P_2^{(m)}$ may be higher than that of $P_2^{(m-1)}$.

One of the experimental tools in the study of mesoscopic samples is a.c. magnetic susceptibility (see e.g. [9,18]). In this technique the response is proportional to the derivative of the average magnetization with respect to the applied flux. The average magnetization is a complicated expression, but among other things, it depends on g . Therefore, the susceptibility diverges as $\Gamma_{\text{II}}^{(m)}$ is approached, and diverges quadratically at $P_2^{(m)}$. This divergence, together with some calculated curves, was obtained in [5] for thin rings. However, it is surprising that the divergence is not smeared in a thick shell, where the “enclosed” flux appears to be poorly defined.

5.4.5 Vortices

Figure 5.8 shows $\mathcal{R}_m(r)$ and $|g|\mathcal{R}_{m+1}(r)$ for a situation in which $\Phi \approx 0.997\Phi_*^{(m)}$. If R_i/R_o is not very small and the flux is not very large, these shapes are typical. ($\mathcal{R}_m(r)$ typically changes from increasing to decreasing as Φ is changed from $\Phi_*^{(m-1)}$ to $\Phi_*^{(m)}$.) As we see from Fig. 5.6, for temperatures higher than that of $P_2^{(m)}$, $|g|$ increases with the flux. This means that, as the flux is increased

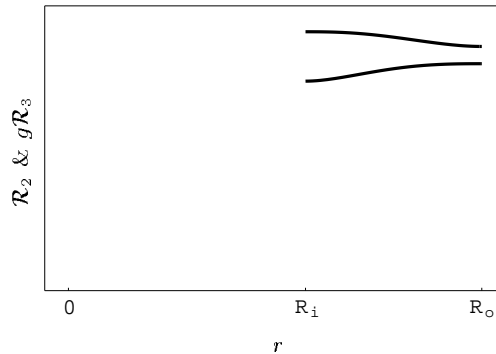


Figure 5.8. Radial dependence of the leading terms in (5.44), including their relative weights, at a flux slightly lower than the degeneracy flux $\Phi_*^{(m)}$. (Here, $|g|\mathcal{R}_{m+1}(r)$ is the lower curve.) In this evaluation we used $m = 2$, $(R_o - R_i)/R_o = 0.426$ and $\epsilon\beta_1 = -0.15$. The “ y -axis” starts from the lower edge of the frame

close to $\Phi_*^{(m)}$, a situation will be reached such that $\mathcal{R}_m(R_o) = |g|\mathcal{R}_{m+1}(R_o)$; for this flux, the leading term in (5.44) vanishes at a point on the outer boundary, at the angle for which $e^{-mi\theta}$ and $ge^{-(m+1)i\theta}$ have opposite phases. As the flux is increased further, the point where $\mathcal{R}_m(r) = |g|\mathcal{R}_{m+1}(r)$ and ψ vanishes will occur in the interval $R_i < r < R_o$. Finally this point reaches the inner boundary and, for still larger fluxes, $|\psi|$ will be positive everywhere [until a flux is reached such that $\mathcal{R}_{m+1}(R_o) = |g|\mathcal{R}_{m+2}(R_o)$]. The point (or actually the line parallel to the magnetic field) where $\psi = 0$ is called a *vortex*.

Figure 5.9 shows the contour plots of $|\psi|$ and the corresponding current densities for $\Phi = \Phi_*^{(0)}$ and for $\Phi = \Phi_*^{(2)}$. In both cases, the darkest region contains a vortex. It is remarkable that for $\Phi = \Phi_*^{(0)}$ the vortex is at the thinnest part of the ring and, for $\Phi = \Phi_*^{(2)}$, at its thickest part. The reason is that $C_0 > 0$, so that it follows from (5.51) that $g < 0$ and the lowest order terms in (5.44) cancel for $\theta = 0$; on the other hand, $C_2 < 0$, so that $g > 0$ and $\psi_0^{(2)} + g\psi_0^{(3)} = e^{-2i\theta}(\mathcal{R}_2(r) + g\mathcal{R}_3(r)e^{i\theta})$ can vanish for $\theta = \pi$. This is a general feature: for low fluxes, $C_m > 0$ and the vortex is located at the thin side, whereas the opposite situation occurs for large m . The values of m for which C_m becomes negative decrease with the relative width of the ring. The last column in Table 5.1 shows the values of w/R_o at which C_m changes sign. C_m does not decrease monotonically with w/R_o ; for a full cylinder ($w/R_o = 1$), $C_m = 0$ for every m . C_0 is always positive (except for $w/R_o = 1$). The effect of the higher order terms in (5.44) is a shift in the position of the vortex by a distance of order ϵ .

We have not found an intuitive argument that explains why the vortex appears at the opposite side of the ring when m crosses the limiting value in Table 5.1, although we have found contradictory handwaving arguments in the literature, unrelated to m . One of them claims that superconductivity should be broken at the thin side, which plays the role of a “defect”. The other argument

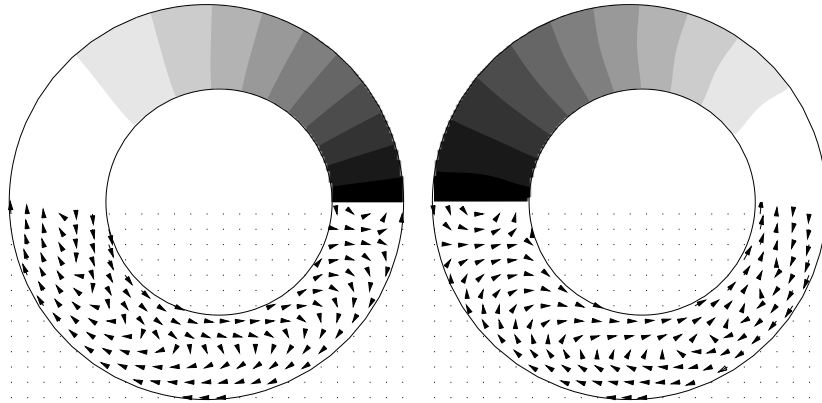


Figure 5.9. The shape of this sample corresponds to $(R_o - R_i)/R_o = 0.426$, $\epsilon\beta_1 = -0.15$; the other harmonics are taken as 0. In the upper half of the sample we show a contour plot of $|\psi|$; in the lower half, the current density field. Left: $\Phi = \Phi_*^{(0)}$; right: $\Phi = \Phi_*^{(2)}$

says that, the thinner a layer, the more it favors surface superconductivity and, therefore, the thin side is the one where superconductivity survives.

According to “common wisdom”, vortices have a core of size of the order of $\xi = \mu^{-1/2}$, and cannot exist in a region which is narrower than this size. This argument can be used to qualitatively explain the upper critical field in type II superconductivity: the density of vortices is H/Φ_0 ; this density cannot be much larger than μ , and therefore there is an upper critical field of the order of $\mu\Phi_0$. For a thin film parallel to the field, its width must be at least $1.8\mu^{-1/2}$ [16] in order to be able to accommodate vortices. For a disk, it is similarly found that its radius has to be at least $1.3\mu^{-1/2}$ in order to contain a vortex. Moreover, old experiments have shown that vortices cannot pass through superconducting bridges which are too narrow.

Contrary to the previous paragraph, our formalism predicts that connectivity can force a vortex to be present in the ring, regardless of its width.

Even if the order parameter does not have axial symmetry, its winding number can still be defined as the integral of its phase, i.e. $(i/2\pi) \oint (\nabla\psi \cdot d\mathbf{r}/\psi)$. However, if there is a vortex in the sample, the value of this integral will depend on the path, being larger by one when the vortex is enclosed than when it is not. At first sight, it might seem impossible to pass continuously from an order parameter with winding number m to another with winding number $m+1$, but, from the previous argument, this is what happens as a vortex moves from the outer to the inner boundary: the set of paths with winding number $m+1$ grows at the expense of the set with winding number m , until it fills the entire sample.

Figure 5.10 is a schematic drawing of the streamlines in the sample, close to a degeneracy flux $\Phi_*^{(m)}$. The figure at the right corresponds to a flux slightly higher

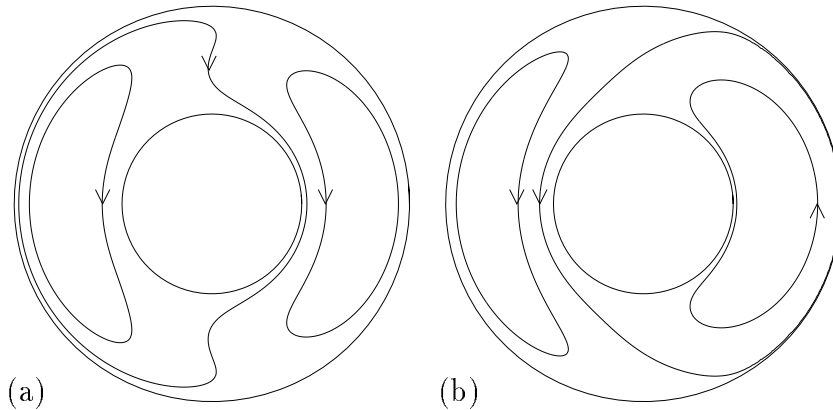


Figure 5.10. Near a degeneracy flux, and provided that the temperature is not much lower than that of P_2 , there are three types of streamlines. At the left side in each figure, we show the screening (clockwise) current. At the right side we show the vortex currents: they surround a point where the order parameter vanishes and the integral of the gradient of the phase is nonzero along these streamlines. For the circulating current (encloses the hole of the sample) there are two possibilities: (a) the vortex is close to the outer boundary, then the circulating current does not enclose the vortex and circulates in the same sense as the screening current; (b) opposite case

than that at the left. There are three distinct classes of streamlines. The circuit at the left in each figure represents the screening (Meissner) currents; the field they induce tends to expel the applied field. The circuit at the right represents the currents around the vortex; they circulate in the paramagnetic sense. The circuit that encloses the hole of the sample represents the current that circulates around the ring. If the vortex is located near the outer (respectively inner) boundary, then the current that circulates around the ring has diamagnetic (respectively paramagnetic) sense. If the flux is not sufficiently close to $\Phi_*^{(m)}$, then the vortex and the currents around it are not present. If the flux is quite apart from degeneracy, then both extremes of the screening circuit merge, giving rise to currents that circulate around the ring, in the diamagnetic (respectively paramagnetic) sense close to the outer (respectively inner) boundary. These paramagnetic and diamagnetic regions are separated by a line where the current vanishes; this line moves inwards as the flux increases, until it reaches the inner boundary and a new screening circuit is formed.

Let us finally consider the case of temperatures lower than that of $P_2^{(m)}$. From Fig. 5.6 we see that, as the flux is increased, an unstable branch will be reached and $|g|$ will increase discontinuously. This means that the vortex will jump inwards. If the discontinuity in g is too large (as is the case for temperatures much lower than that of $P_2^{(m)}$) the winding number will jump from m to $m + 1$, without the presence of any vortex in the sample.

5.4.6 Inhomogeneous Fields

If the applied field is not uniform, but does have cylindric symmetry, we can still use the formalism exposed at the opening of Section 5.4, and (5.27) is still valid. In the present case

$$A(r) = \frac{1}{r} \int_0^r H_e(r') r' dr' . \quad (5.55)$$

In general, (5.27) is an ordinary eigenvalue differential equation and can be solved numerically. However, we consider below a few cases in which analytic treatment may be useful.

Zero Field through the Sample In this case, the magnetic potential in the sample is due only to the flux $\phi\Phi_0$ enclosed within the hole $r < R_i$ and $\tilde{A}(r) = \phi/r$ for $R_i \leq r \leq R_o$. This leads to

$$\mathcal{R}_m(r) = k_J J_{|\phi-m|}(\sqrt{\mu}r) + k_Y Y_{|\phi-m|}(\sqrt{\mu}r) , \quad (5.56)$$

where $J_*(.)$ (respectively, $Y_*(.)$) is the Bessel function of the first (respectively, second) kind and the eigenvalue μ and the ratio k_J/k_Y are such that the Neuman condition is fulfilled. Since m enters (5.56) only through $|\phi - m|$, it follows that \mathcal{R}_m and \mathcal{R}_{m+1} have the same eigenvalue for $\phi = m + 1/2$. This means that $\Phi_*^{(m)} = (m + 1/2)\Phi_0$, as in the case of a thin shell. Moreover, \mathcal{R}_m and \mathcal{R}_{m+1} become identical for $\Phi = \Phi_*^{(m)}$. Their common expression can be written in the form

$$\mathcal{R}_* = (k_J \sin(\sqrt{\mu}r) + k_Y \cos(\sqrt{\mu}r))/\sqrt{r} . \quad (5.57)$$

Instead of the case of Fig. 5.8 we have a new scenario: as $|g|$ increases from the situation with winding number m to that with winding number $m + 1$, \mathcal{R}_m and $|g|\mathcal{R}_{m+1}$ will not become equal at a single point, but rather for all r in the sample. This means that instead of a vortex there will be a *cut* with vanishing ψ across the sample, from the inner to the outer boundary, i.e. the superconducting region becomes singly connected, as we found in the one-dimensional problem. This is a particular case of Theorem 4 in Chapter 3.

Piecewise Constant Field Let us now consider a magnetic field of the form

$$H_e(r) = \begin{cases} h_1 & r \leq R_M \\ h_2 & r > R_M \end{cases}$$

with $R_i < R_M < R_o$.

Following (5.55), for $r \leq R_M$ we recover the case of a homogeneous field $H_e = h_1$; for $r > R_M$ we obtain the same form as for $H_e = h_2$, but m has to be replaced with $m - \phi_M$, where $\phi_M\Phi_0$ is the flux of a field $h_1 - h_2$ through a disk of radius R_M . At $r = R_M$, we require continuity of \mathcal{R}_m and \mathcal{R}'_m .

Figure 5.11 shows \mathcal{R}_m and $|g|\mathcal{R}_{m+1}$ for a case $h_2 = -h_1$. The sign reversal of the magnetic field causes a reversal in the growing trends of \mathcal{R}_m and $|g|\mathcal{R}_{m+1}$

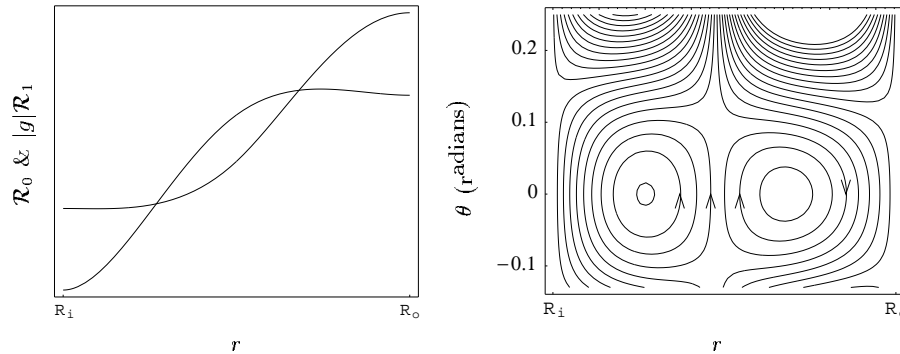


Figure 5.11. Left: Radial dependence of the leading terms in (5.44), for a case in which the magnetic field switches sign at $r = R_M$. The “ y -axis” starts far below the lower edge of the frame. Right: Streamlines at a radial strip of the sample, close to $\theta = 0$. (If the first harmonic is dominant, this is the region where the sample is narrowest.) Along the line $\theta = 0$ there is a vortex (respectively, antivortex) at the side close to the inner (respectively, outer) boundary. For $\theta \gtrsim 0.15$, the screening currents are seen; again, their sense depends on the direction of the local field. For these figures we have used $(R_o - R_i)/R_o = 0.426$ and $R_M = (R_i + R_o)/2$; the degeneracy between winding numbers 0 and 1 occurs when the flux through $r \leq R_M$ is $0.684\Phi_0$

and as a result, for $|g|$ in the appropriate range, $|g|\mathcal{R}_{m+1}(r) > \mathcal{R}_m(r)$ far from the boundaries and the opposite holds near the boundaries. This means that we have a different scenario than in Fig. 5.8, since now ψ vanishes at two points. For paths which enclose the hole of the sample and cross the line $\theta = 0$ between these two points, the winding number is $m + 1$; for paths that cross $\theta = 0$ skipping the line between these two points, the winding number is m . The currents around the inner point where ψ vanishes induce a positive field at it, as usual in vortices; the currents around the outer point induce a negative field and we call this point an *antivortex*.

In summary, as $|g|$ increases, a vortex - antivortex pair appears in the middle of the sample $R_i \leq r \leq R_o$ and then the vortex moves towards the inner boundary while the antivortex towards the outer one, until $|\psi| > 0$ everywhere and the winding number is $m + 1$ for every path.

Thin Shells If $(R_o - R_i) \ll R_o$, we can write the flux as the sum of the contribution from the regions inside and outside R_i , and treat the latter as a perturbation. For example, it is interesting to find a condition for the field at which the degeneracy of m and $m + 1$ occurs. Writing $\tilde{A} = (m + 1/2 + \phi_1(r))/r$, the condition for degeneracy, to first order perturbation and for linearized GL, is

$$\int_{R_i}^{R_o} \frac{\phi_1(r) \mathcal{R}_*^2 dr}{r} = 0, \quad (5.58)$$

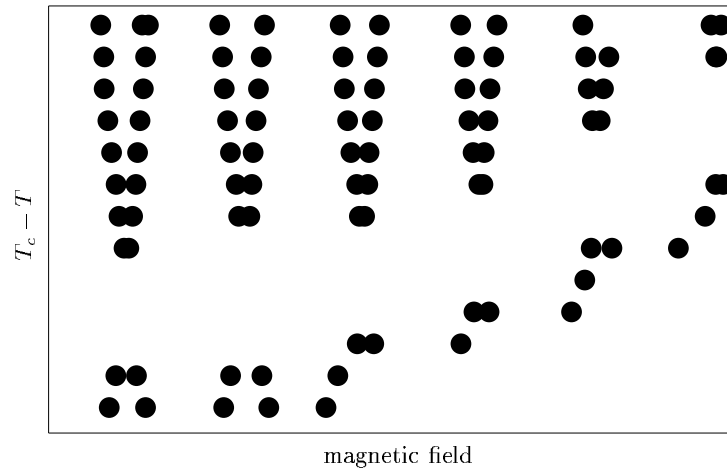


Figure 5.12. Experimental phase diagram [10]. The lower points indicate the normal/superconducting transition; the points at the left (respectively, right) of the “V”-shaped formations show the stability limit of the state with winding number $m + 1$, where it decays into m (respectively, decay from m to $m + 1$). In this experiment, $w/R_o = 0.38$ and β_1 is unknown

where \mathcal{R}_* was defined in (5.57). As a test to (5.58) we have applied it to the degeneracy field of Fig. 5.11 (in spite of the fact that the considered shell is not thin). We obtain

$$\int_{R_i}^{R_o} \frac{\phi_1(r) \mathcal{R}_*^2 dr}{r} \bigg/ \int_{R_i}^{R_o} \frac{|\phi_1(r)| \mathcal{R}_*^2 dr}{r} = -3.6 \times 10^{-6} .$$

5.4.7 Experimental and Numerical Evidence

Experimental Phase Diagram Kanda *et al.* [10] obtained the phase diagram for a mesoscopic Al ring (Fig. 5.12), by means of voltage-induced tunneling measurements. The ring was intended to have uniform cross section, but, clearly this is never perfectly true in a real experiment. As far as one could expect, their result is in agreement with Fig. 5.5: close to the onset of superconductivity (Γ_1), there is a continuous passage between consecutive winding numbers, whereas far from Γ_1 the passage is discontinuous and hysteretic.

ac Susceptibility For narrow rings, the ac susceptibility is proportional to the derivative of the current with respect to the flux. Zhang and Price [17] measured the ac susceptibility for a mesoscopic Al ring. As in the previous case, the ring was intended to have uniform cross section. Again, they found continuous passage between m and $m + 1$ close to Γ_1 and hysteretic behavior far from this line. Moreover, they found magnetic signatures of the critical points $P_2^{(m)}$. Close to

Γ_1 , the passage between winding numbers shows paramagnetic ac susceptibilities, as predicted. This feature was discussed in [5]; note, however, that for a wide ring as used in this experiment, evaluation of the induced flux as being due to the current around the ring may not be a good approximation, and the contributions of the entire current distribution ought to be taken into account.

The divergence of the ac susceptibility at $P_2^{(m)}$, predicted at the end of Section 5.4.4, is consistently found. In Fig. 5.13 we show the ac susceptibility for the temperatures at which this divergence appears. We emphasize that these are precisely the limiting temperatures between the continuous and hysteretic regimes for each m . Setting $w/R_o = 0.426$ (as reported in this experiment) in Fig. 5.7, we obtain that the values of μ at $P_2^{(0)}$, $P_2^{(1)}$ and $P_2^{(2)}$ are in the ratio 1:1.4:2.8 for a deviation from axial symmetry $|\beta_1| = 0.15$. (In the experiment, $|\beta_1|$ was not determined.) The ratios among the values of μ are to be compared with those of the temperatures of the experimental candidates for $P_2^{(m)}$, measured from T_c . Taking the reported value $T_c = 1.266$ K, these temperature differences are in the ratio 1:1.5:2.0, in semiquantitative agreement with theory.

Far from Axial Symmetry The case of a sample with cylindric eccentric boundaries was treated in [7], using linearized GL and a variational approach. The same scenario obtained here near axial symmetry, shows up for large eccentricity. For small winding numbers, vortices pass through the sample across its thinnest part, whereas for large m they pass across the opposite side. For a sample with relative width $(R_o - R_i)/R_o = 0.31$, the first vortex that crosses through the thickest side occurs for the passage from $m = 3$ to $m = 4$. According to Table 5.1, this is expected for relative width in the range $0.22 \leq (R_o - R_i)/R_o \leq 0.29$, indicating that eccentricity tends to lower the effective relative width.

The results obtained in this section are based on the assumption that the induced potential can be neglected. This is expected for $\mu h(R_o - R_i)\kappa^{-2} \ll 1$ in the case of thin samples, or $\sqrt{\mu}(R_o - R_i)/\kappa \ll 1$, in the case of long samples. In the opposite extreme, we expect bulk behavior, i.e. Meissner or Abrikosov state. We would like to have an estimate for the value of $\mu h(R_o - R_i)\kappa^{-2}$ at which our scenario breaks down. This is provided by the results of Baelus *et al.* [1]. They also considered disks with a circular hole at an asymmetric position, but used the entire GL equations, which they solved numerically.

In one of their examples, $\mu h(R_o - R_i)\kappa^{-2} \sim 0.1$. They did obtain hysteresis at the transition between $m = 0$ and $m = 1$, which at the temperature they considered is far from the superconductivity onset, and did not find hysteresis for the transitions at higher m (which are closer to Γ_1 ; see Fig. 5.5). For the continuous transitions ($m \geq 1$), they always found the vortex at the thick side of the ring, as expected from Table 5.1 and their ratio $(R_o - R_i)/R_o = 0.75$. For large eccentricity, the transition between $m = 0$ and $m = 1$ becomes continuous; in this regime the vortex is found at the thin side of the ring [12], again as expected. Surprisingly, for large eccentricity the transition between $m = 1$ and $m = 2$ becomes discontinuous. Apparently, the effective relative width is reduced to values close to 0.44, so that $C_1 \sim 0$ and the anomalous situation

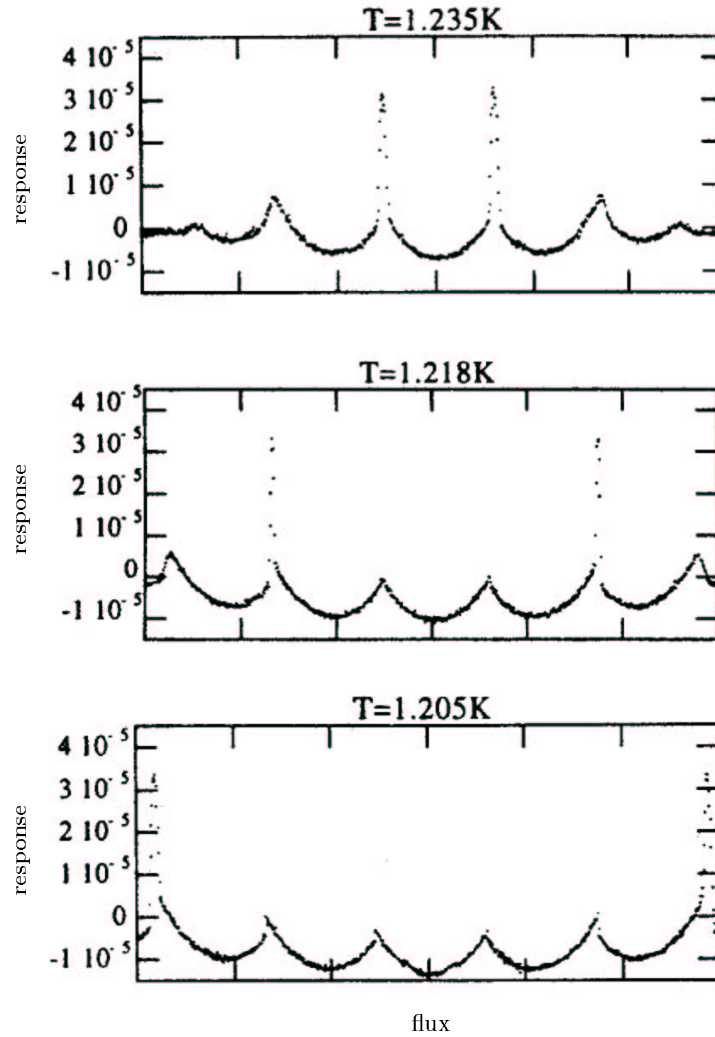


Figure 5.13. ac susceptibility (which is proportional to the experimental “response”) as a function of the flux. Each temperature corresponds to the limit between continuous and discontinuous transitions between consecutive winding numbers, $0 \leftrightarrow 1$, $1 \leftrightarrow 2$ and $2 \leftrightarrow 3$. The flux vanishes in the middle of the graphs and every tick corresponds to Φ_0 through the average radius of the sample. (Taken from Ref. [18]; $w/R_o = 0.426$). Note that, in each graph, for winding numbers lower (respectively, higher) than those involved in the divergence, the transition is discontinuous (respectively, continuous)

discussed in p. 153 is encountered. This situation could be checked by varying the temperature: if $C_1 \sim 0$, $\Gamma_{II}^{(1)}$ and Γ_I should be very close to each other.

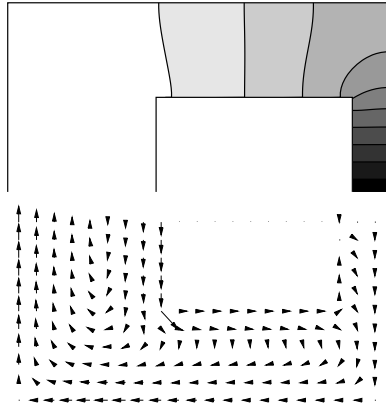


Figure 5.14. Numerically evaluated contour plot of $|\psi|$ and field plot of the current density. There is a vortex in the middle of the narrow branch. Most of the current is screening current, but a few arrows are seen around the vortex and the circulating current is seen in the counterclockwise sense along the inner boundary. Here each outer edge equals 1.27 coherence lengths, the flux enclosed by the outer boundary is $1.07\Phi_0$ and $\kappa = 0.4$

For their example with $\mu h(R_o - R_i)\kappa^{-2} \sim 0.2$, *two* vortices appear simultaneously, indicating that our formalism is no longer valid.

Non Smooth Boundaries We have studied the case of a long (i.e. independent of z) sample with eccentric squared boundaries. Half of its cross section is shown in Fig. 5.14. The GL equations were solved numerically, by means of the program described in Chapter 8. This time the induced potential was not neglected. The results are qualitatively the same as for the case of circular boundaries. Far from the superconducting/normal transition, the winding number changes hysteretically as the magnetic field is swept, whereas close to this transition the change is mediated by the continuous passage of a vortex. When the winding number changes from 0 to 1, or from 1 to 2, the vortex passes through the thin part of the sample; when the winding number changes from 2 to 3, the vortex passes through the thick part. Making the natural identification of $R_{i,o}$ as a length proportional to the respective perimeter, the studied sample obeyed $(R_o - R_i)/R_o = 1/2$; according to Table 5.1 the effective value of $(R_o - R_i)/R_o$ was somewhat lower, as in the case of eccentric circular boundaries.

The shape of the magnetization we found is similar to that in Fig. 20b in [1]. The maximum of the magnetization is not necessarily found at the first ($m = 0$) peak.

The presentation of Fig. 5.14 suggests that $|\psi|$ and the current have the same mirror symmetry as the sample. For the magnetic fields at which there was a vortex in the sample, this appeared to be indeed the case, but in general, this does not seem to be true.

5.4.8 Josephson Junctions

In this section we have considered the situation where $T \sim T_c$ and, in addition, the shape of the sample is not extremely far from a uniform cross section. We shall now review the opposite situation: $T \ll T_c$ and the sample contains a “weak link”, which is the only segment where the current density is not zero in the interior of the sample. This weak link is called a Josephson junction; the structure which consists of a loop with a weak link is called “rf-SQUID”, and was studied long ago [11].

The behavior of the rf-SQUID is basically the same as that obtained in Section 5.4.4: there are two possible regimes, one with continuous and the other with discontinuous passage between consecutive winding numbers. However, whereas in Section 5.4.4 the requirement for continuous passage is a low value of $\mu_1/(|\beta_1|\mu_P^{(m)})$ [this can be obtained from (5.54), estimating A_m, B_m, C_m , etc. from their definitions], in the rf-SQUID case the condition is $2\pi LJ_c \leq \Phi_0$, where L is here the self-inductance of the loop and J_c the maximum current which can pass through the junction.

Increasing $|\beta_1|$ produces a narrower constriction at the thin side of the ring and, therefore, a lower possible current through this constriction. In this sense, J_c may be regarded as a continuation of the effect provided by $1/|\beta_1|$. A large value of $\mu_1/\mu_P^{(m)}$ means strong superconductivity and hence, large J_c . In this sense, J_c may also be regarded as the continuation of the influence of the ξ -dependence of μ_1 . However, the rf-SQUID is not influenced by the length of the loop, whereas $\mu_P^{(m)} \propto R_o^{-2}$. This comparison suggests that, once the perimeter is much larger than the coherence length, its precise value is not important. At the other extreme, near the onset of superconductivity, the induced field is negligible and thus the self-inductance is unimportant.

It would be interesting to have a study that bridges between these two extreme situations.

5.5 Main Conclusions

A mesoscopic superconducting ring exhibits qualitatively different behaviors, depending on whether it has or does not have an axis of rotation symmetry. This difference shows up for magnetic fields in ranges close to the degeneracy fields, at which the energies of states with consecutive winding numbers coincide.

We have mostly studied the case of samples with an eccentric hole. In this case and near the onset of superconductivity, the state of the sample can pass continuously from a given winding number to the next. This occurs by means of a vortex which crosses the sample. This vortex may cross either through the thinnest or through the thickest part the sample, depending on the winding number and on the ratio between the width and the sample radius. Table 5.1 tells us which scenario occurs.

An additional feature, is the existence of the critical point P_2 , discussed in Section 5.4.4. At P_2 , the magnetic susceptibility diverges quadratically.

Several predictions stem from the present study, and they cry out for experimental verification. The experiments reviewed in Section 5.4.7 were not designed to check the present predictions. Rather, they were intended to check unrelated aspects of the ideal case where there is axial symmetry, and the qualitative agreement with our predictions was revealed by accident, thanks to experimental imperfections.

The feature which seems to be the most easily measurable is the magnetic susceptibility near P_2 . This has been done by means of SQUID microsusceptometry [17,18] and experimentally equivalent situations have been coped with by means of ballistic Hall junctions [9]. A possibility which seems especially attractive would be to measure the magnetization of half of the sample, since this could reveal in which half the vortex is found.

In order to measure the order parameter directly, the most appropriate technique seems to be scanning tunneling microscopy/spectroscopy. It is hard to use this technique in Al (which is popular in the fabrication of mesoscopic samples, due to its large coherence length). However, successful measurements have been performed in In disks. It is also possible to measure the superconducting gap at fixed tunneling points, as in [10]. In this experiment, there were only two contact points, so that no information was obtained on the shape of the order parameter. If the same kind of experiment were repeated with several leads, the shape of the order parameter could be mapped.

Acknowledgements

I wish to thank Akinobu Kanda for sending me the data for Fig. 5.12, Gustavo Buscaglia for sending me the computer program used for the case of squared boundaries, John Price for sending me Xianxian Zhang's thesis and unpublished data, and François Peeters for sending me unpublished results.

References

1. B. J. Baelus, F. M. Peeters, V. A. Schweigert: Phys. Rev. B **61**, 9734 (2000)
2. R. Benoist, W. Zwerger: Z. Phys. B **103**, 377 (1997)
3. J. Berger: Physica C, in press
4. J. Berger, J. Rubinstein: Physica C **288**, 105 (1997)
5. J. Berger, J. Rubinstein: Phys. Rev. B **56**, 5124 (1997)
6. J. Berger, J. Rubinstein: SIAM J. Appl. Math. **58**, 103 (1998)
7. J. Berger, J. Rubinstein: Phys. Rev. B **59**, 8896 (1999)
8. E. H. Brandt: Phys. Rev. B **58**, 6506 (1998)
9. A. K. Geim *et al.*: Appl. Phys. Lett. **71**, 2379 (1997); A. K. Geim, S. V. Dubonos, J. G. S. Lok, M. Henini, J. C. Maan: Nature **396**, 144 (1998)
10. A. Kanda, M. C. Geisler, K. Ishibashi, Y. Aoyagi, T. Sugano: Physica B, in press
11. O. V. Lounasmaa: *Experimental Principles and Methods Below 1K*. (Academic, London 1974)
12. F. Peeters: unpublished
13. G. Richardson: Quart. Appl. Math., in press

14. J. Rubinstein: 'Six lectures on superconductivity'. In: *Proc. of the CRM Summer School on Boundaries, Interfaces and Transitions*, ed. by M. Delfour (American Mathematical Society, 1998) pp. 163-184
15. J. Rubinstein, M. Schatzman: *J. Math. Pure Appl.* **77**, 801 (1998)
16. D. Saint-James, G. Sarma, E. J. Thomas: *Type II superconductivity* (Pergamon, Oxford 1969)
17. X. Zhang, J. C. Price: *Phys. Rev. B* **55**, 3128 (1997)
18. X. Zhang: SQUID Microsusceptometry of Mesoscopic Superconducting Rings. PhD Thesis, University of Colorado, Boulder (1996)